Electrical Impedance Tomography for Artificial Sensitive Robotic Skin: A Review

David Silvera-Tawil, *Member, IEEE*, David Rye, *Member, IEEE*, Manuchehr Soleimani, and Mari Velonaki

Abstract—Electrical impedance tomography (EIT) is a nondestructive imaging technique used to estimate the internal conductivity distribution of a conductive domain by taking potential measurements only at the domain boundaries. If a thin electrically conductive material that responds to pressure with local changes in conductivity is used as a conductive domain, then EIT can be used to create a large-scale pressure-sensitive artificial skin for robotics applications. This paper presents a review of EIT and its application as a robotics sensitive skin, including EIT excitation and image reconstruction techniques, materials, and skin fabrication techniques. Touch interpretation via EIT-based artificial skins is also reviewed.

Index Terms—Robot skin, electrical impedance tomography, robot sensing systems, tactile sensors, human-robot interaction.

I. INTRODUCTION

OVER the last decade the field of robotics has seen a significant increase in human-robot interaction (HRI) research [1]. As robots begin to be deployed outside engineered factory environments and the distance between humans and robots narrows, there is an increasing need for robots to have capabilities that will allow them to interact fluently and intuitively with humans [2]. Although significant progress has been made in the area of audio-visual communication [3], until recently the field of touch has been significantly neglected.

During social interaction humans extract important information from tactile stimuli that helps them understand the meaning of the interaction. A similar capability in a robot will allow for safe, natural and intuitive interactions between humans and robots. In robotics, it is therefore important to design a method for touch identification that can be active over all or most of the surface of a robot, including large curved robot surfaces. This could be achieved using an artificial "sensitive skin" [4].

In the literature an artificial sensitive skin for robotics applications is usually considered to be a large, flexible [5], [6] and stretchable [7] array of sensors that can be used to cover

various three-dimensional robotic surfaces, including three-dimensionally curved and movable parts. It is often assumed that the number of sensors distributed over the artificial skin should be large and that the sensors should be small, especially on hands and fingers [8]. Sensors should be light-weight, robust, stable, replicable, and capable of detecting a wide range of information [7], [9]. In some cases, multiple layers of heterogeneous sensors [10] are used in an attempt to more closely imitate the capabilities of human skin [11], [12].

Skin fabrication should be simple, low-cost, replicable, scalable and result in durable skin. Electronics should be designed for minimum power consumption and be suitable for battery-powered operation. All sensing capabilities should remain the same regardless of the position of the robot, joint movement, or skin stretch. All hardware should be designed to withstand settings and environments suitable for humans. The reader is referred to [7]–[9] and [13] for more detailed requirements.

Electrical impedance tomography (EIT) [14] is a non-destructive imaging technique used to estimate the internal conductivity distribution of an electrically conductive body by using measurements from electrodes attached only to its boundary. If this body is made of a thin, flexible and stretchable material that responds to touch with local changes in conductivity, it can be used to create an artificial sensitive skin for robotics applications. The application of EIT to robotic skin was first described by Kato et al. [15] and Nagakubo et al. [16] who placed electrodes on the border of a rubberised material that responded to applied pressure with local changes in resistivity. Changes in resistance—and therefore pressure—were identified by applying EIT. A limited number of measurement electrodes can be also placed inside the borders of the conductive material [17].

Since most of the sensing area in EIT-based artificial skins is made of a homogeneous thin material without any (or very limited) internal wiring, a large, flexible and stretchable artificial skin can be created. Because EIT-based sensitive skins are made of a single material, as opposed to multiple discrete sensors interconnected in an array configuration [18], they are able to provide continuous sensing. Furthermore, since the response of the system depends on the localised conductivity changes of the variable-conductance material in response to an external stimulus, materials sensitive to different types of stimuli, such as temperature, could be used to sense other types of excitation. An EIT-based sensitive skin has the potential to provide a low cost, easy-to-manufacture solution to the

TABLE I

SUMMARY AND COMPARISON OF VARIOUS TOUCH-BASED SENSING TECHNIQUES

Type	Sensing Principle	Advantages	Disadvantages
Capacitive [26], [27], [49]–[52]	Change in capacitance	Excellent sensitivity; good spatial resolution; large dynamic range.	Stray capacitance; noise susceptibility; complexity of measurement electronics.
Piezoresistive [19], [53]–[57]	Change in resistance	High spatial resolution; structured sensors; high scanning rate; low cost.	Low repeatability; high hysteresis; high power consumption; fragile; noise susceptibility.
Strain gauges [58], [59]	Change in resistance	Large sensing range; high sensitivity; low cost; simple calibration.	Susceptible to humidity and temperature changes; complex design; non-linearity; susceptible to EMI induced errors.
Optoelectric [39], [40], [60]–[63]	Light intensity and/or spectrum change	Good sensing range; good reliability; high repeatability; high spatial resolution; immune to EMI; rapid response.	Bulky in size; non-conformable; high power consumption.
Piezo-electric strain (stress) polarisation [34]–[36], [64]–[67]	Strain (stress) polarisation	High frequency response; high sensitivity; high dynamic range.	Poor spatial resolution; dynamic sensing only; susceptible to temperature changes.
Inductive/Magnetic [28], [29], [68]–[70]	Change in magnetic coupling	Linear output; high dynamic range.	Moving parts; low spatial resolution; bulky; highly susceptible to noise.
Multi-component sensors [20], [71]–[73]	Coupling of multiple intrinsic parameters	Ability to overcome certain limitations via combination of intrinsic parameters; discrete assembly.	High assembly costs.
Electrical Impedance Tomography [16], [17], [74]–[77]	Change in electrical impedance	Scalable; versatile; low cost; low power consumption; no mechanical parts; no internal wiring in sensing pad; conformable; design simplicity; low assembly costs; good sensing range; good reliability; high repeatability; immunity from EMI.	Low spatial resolution; low temporal frequency.

problem of flexible and stretchable large-scale touch sensing.

Following this introductory section, Sec. II presents an introduction to artificial skin for robotics applications. Sec. III then gives a general overview of EIT: the forward problem, inverse solution, regularisation methods and image reconstruction. Details on how EIT has been used for the development of a robotics skin are presented in Sec. IV. Skin evaluation and performance metrics are introduced in Sec. V. Touch interpretation via an EIT-based sensitive skin is discussed in Sec. VI, which is followed by a discussion and conclusions in Sec. VII.

II. ARTIFICIAL SENSITIVE SKIN FOR ROBOTICS

Since the introduction of the concept of "artificial sensitive skin" for robotics [4], a number of skin prototypes have been created. These prototypes are commonly made of a discrete number of sensors connected individually or in an array configuration [19] and capable of measuring a range of physical phenomena such as pressure, vibration and temperature [20].

A number of different technologies have been used in endeavours to create better tactile sensors and sensitive skins. A wide variety of sensing techniques has stemmed from exploration of different transduction effects and materials, ranging from the use of large-scale arrays of discrete sensors based on organic FETs [21] or piezoresistive semiconductors [22]–[24] to sensors that use capacitive [25]–[27], magnetic [28], [29], piezoelectric [30]–[36], optical [37]–[40] and other principles [41]–[43]. Often, multiple layers of different sensor types [18] are used in an attempt to imitate the sensing capabilities of human skin [11]. Table I summarises and compares various touch-based sensing techniques; similar tables can be found in [8] and [44]. A comprehensive description of various tactile sensor types can be found in [45]–[48], studies of the state-of-the-art in tactile sensing and artificial skin for robotics and biomedical applications are given in [7], [8], and [13], and a review of artificial skin and tactile interaction in socially-interactive robots is presented in [9].

Commonly, the number of wires required to transmit data from large-scale arrays of sensors constitutes a problem in itself. A large number of distributed wires is not only an excellent antenna for electromagnetic noise, but the wires can reduce the flexibility and stretchability of the skin to levels that may impede the dexterity of the robot. EIT-based touch sensors were introduced partially in response to this issue.

EIT-based sensors were first described in 2007 in [15] and [16]. In this method, electrodes are located on the border of a thin sheet of conductive material (such as rubber, foam or fabric) that responds to localised pressure with local changes in conductivity. EIT can then be used to determine the changes in conductivity—as a result of pressure changes—across the material. Since these sensors are constructed from flexible and even stretchable materials without any—or very limited—internal wiring, it is possible to create artificial skins of arbitrary size and shape. As shown in Table I, EIT-based pressure sensors overcome the disadvantages of most conventional sensing methods. Major disadvantages, however, are their relatively low spatial and temporal resolutions, and limited ability to discriminate between pressure intensities and contact areas. As a result, EIT-based artificial skins are not suitable for applications where reconstructions at high temporal frequencies and millimetric spatial resolutions, such as texture recognition [78] and object manipulation [79], are needed. The approach is, however, suitable for a wide range of real-time distributed pressure monitoring applications, including gait detection

in biomechanics [71], [80]. In robotics, EIT-based artificial skins are suitable for touch sensing for safety and human-robot interaction purposes, where spatial resolutions of 10–40 mm and reconstruction frequencies of up to 45 Hz are adequate [81]–[84]. The following section describes EIT and how it can be used in the development of large-scale skin-like sensors for touch sensing in robotics applications.

III. ELECTRICAL IMPEDANCE TOMOGRAPHY FOR SENSITIVE SKIN APPLICATIONS

The practice of using electrical impedance tomography (EIT) as a non-destructive technique to infer the internal conductivity characteristics of a body was first suggested by Henderson and Webster [85] in their work on medical imaging, and by Lytle and Dines [86] in the field of geophysical imaging. Since then EIT has been used in a number of areas such as geophysical exploration [87], [88], industrial applications [89]–[91], biomedical imaging [14], [92]–[98], and most recently in robotics for sensitive skin applications [15]–[17], [75], [84].

In a typical EIT application, multiple electrodes are placed equidistantly around a conductive body (e.g. a person's thorax) and a small alternating current (0.1–1 mA at 10–100 kHz in humans) is applied across two of the electrodes. Consequently, current will flow not only between the source and sink electrodes, but also within the whole conductive body. The potentials at all electrodes resulting from the applied current are measured. Local variations in the internal impedance of the body will alter the distribution of current inside the body, resulting in changes of potential on the boundary. By scanning around various driving electrode pairs and applying an imaging technique, the approximate distribution of current within the conductive body can be calculated through an inverse solution of Maxwell's equations. If direct current (DC) is used instead of alternating current (AC) and the same method is applied to measure only conductivity changes, the technique is referred to as electrical resistance tomography.

The first practical method for EIT reconstruction was back-projection [92], [99], a linear, non-iterative method in which the equipotential volume between a pair of electrodes is back-projected along the whole boundary of the body. This method is similar to X-ray computed tomographic (CT) reconstruction, with the main difference being that in EIT current does not move in a straight line but floods a region from source to drain, as shown in Fig. 1. Although back-projection was very successful for simple two-dimensional geometries, a number of deterministic algorithms based on the Jacobian of the discrete forward solution have been introduced [100]–[103]. This Jacobian is the linearised mapping from boundary potential to internal conductivity.

The EIT reconstruction problem of finding an internal conductivity distribution of a body when a set of injected currents and measured potentials is known is mathematically an ill-posed non-linear inverse problem in which the aim is to find the cause given the effect. According to Hadamard [105] a problem is well-posed if: (1) for all data a solution exists; (2) the solution is unique; and (3) the solution depends continuously on the data. In this sense, the problem of recovering

(a) X-ray computed tomography (CT).

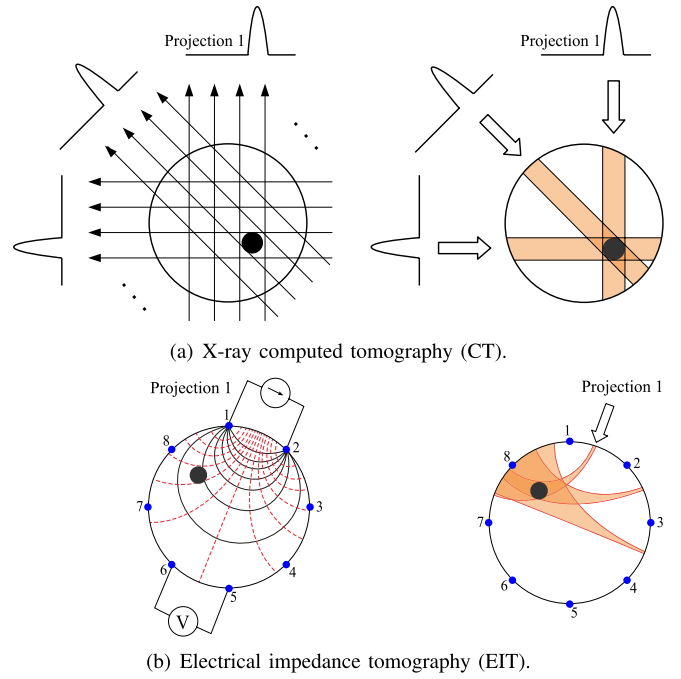(b) Electrical impedance tomography (EIT).

Fig. 1. Principle of back-projection for X-ray CT and EIT reconstructions. Red (dashed) lines in (b) represent the likely equipotential lines. Orange regions in (a) and (b) represent the volume projected during three scanning steps. Part (a) adapted from Dai [104]. Current paths in (b), represented by the black solid lines, are diagrammatic only.

the internal conductivity given a set of potentials on the boundary is strongly ill-posed. Even if some conditions are assured to guarantee the existence of a solution (Hadamard's criteria 1 and 2), the EIT reconstruction problem fails the third criterion: small changes at the boundary (e.g. electrical noise on the electrodes) can result in large, unpredictable changes in the reconstructed image.

A common approach to solving this kind of numerically ill-posed problem is to add some prior information to the solution and thereby replace the original problem with a nearby well-posed problem. This technique is known as *regularisation*. The remainder of this section briefly describes the EIT forward and inverse problems, forward solution, regularisation and inverse solution, and how they can be used to effect an artificial skin sensitive to touch.

A. The EIT Forward Problem

The starting point for the solution of the EIT forward problem is Maxwell's equations for electromagnetism [14]. For a conducting domain Ω with boundary $\partial\Omega$ and known conductivity distribution σ, the forward problem is to find the potentials on the boundary due to the given currents injected through the boundary. The mathematical model can be derived by solving the Laplacian elliptic partial differential equation

$$0 = \sigma \nabla^2 u \quad \text{in} \ \ \Omega, \tag{1}$$

which describes the steady-state conductivity distribution in the absence of current sources and sinks within the domain Ω.

In a practical EIT application, current is injected (sourced and sunk) through electrodes attached to the boundary $\partial\Omega$ of
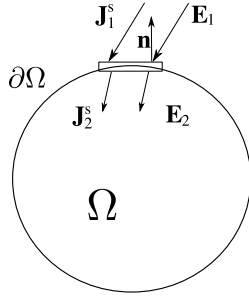
Fig. 2. EIT boundary conditions: $\mathbf{J}_1^s$ and $\mathbf{J}_2^s$ are, respectively, the current source densities outside and inside the domain; $\mathbf{E}_1$ and $\mathbf{E}_2$ are the corresponding electric fields. Adapted from [100].

the domain, as shown in Fig. 2. Assuming that there are no current sources inside the domain ($\mathbf{J}_2^s = 0$) and no electric fields outside the domain ($\mathbf{E}_1 = 0$) then

$$-\sigma \mathbf{E} \cdot \mathbf{n}|_{\text{inside}} = -\mathbf{J}^s \cdot \mathbf{n}|_{\text{outside}}$$

holds, where $\mathbf{n}$ is the unit normal to the boundary $\partial\Omega$. By applying the Neumann boundary condition to the Laplacian (1) we obtain

$$\sigma \frac{\partial u}{\partial \mathbf{n}} = -\mathbf{J}^s \cdot \mathbf{n} \equiv j \quad \text{on} \ \ \partial\Omega, \tag{2}$$

where u is the electric potential and j is the inward-pointing normal component of the injected current density $\mathbf{J}^s$ on the boundary. Full derivations of the boundary condition are presented by Vauhkonen [100] and Noor [106]. For the remainder of this document j will be referred to as the injected current.

To complete the mathematical model it is necessary to determine an appropriate electrode model that takes into account the effects of current injection and potential measurement through the electrodes. The simplest model is the *continuum model* [96]. This model assumes that the injected current j is a continuous function, without considering the influence of any discrete electrodes present on the boundary. The continuum model considers the Laplacian (1) and the boundary condition (2), together with a conservation of charge condition

$$\int_{\partial\Omega} j = 0 \quad \text{and} \quad \int_{\partial\Omega} u = 0,$$

which amounts to choosing a reference voltage or "ground".

In a practical application, however, current is injected through a discrete number L of finite electrodes attached to the boundary. The *gap model* [100] takes into account the existence of these electrodes and assumes that the total injected current j is

$$j = \frac{I_l}{|e_l|} \quad \text{on} \ \ e_l, \quad l = 1, 2, \ldots, L \tag{3}$$

within the electrode and zero elsewhere. Here I_l is the current injected at the l'th electrode and $|e_l|$ is the electrode contact area, or length for the two-dimensional case.

Alternatively, the *shunt model* [96], [100] takes into account the fact that the potential V_l measured across the l'th electrode is constant across the highly-conductive electrode:

$$u = V_l \quad \text{on} \ \ e_l, \quad l = 1, 2, \ldots, L,$$

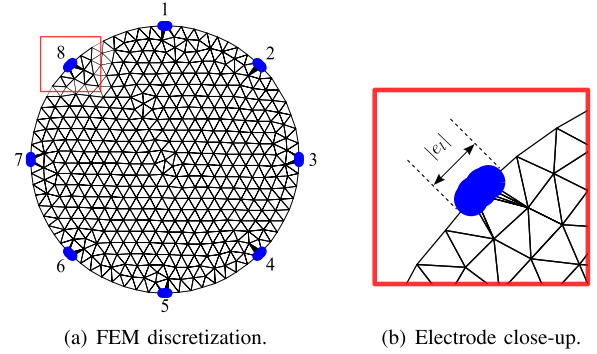(a) FEM discretization.   (b) Electrode close-up.

Fig. 3. Finite element discretization for a circular two-dimensional domain formed by a finite number of triangles. Filled blue circles mark the nodes associated with electrode positions. The electrode close-up in (b) shows the use of multiple nodes to represent the length of the electrode as required by the complete electrode model. The FEM mesh was generated using DistMesh [111].

and the boundary condition (2) is exchanged for one that requires the current density over the surface s of an electrode to equal the current I_l flowing through the electrode

$$\int_{e_l} \sigma \frac{\partial u}{\partial \mathbf{n}} ds = I_l \quad \text{on} \ \ e_l, \quad l = 1, 2, \ldots, L. \tag{4}$$

Finally, the *complete electrode model* [96], [100] considers the existence of a discrete number of electrodes of finite size (gap model), the shunting effect of a conductive electrode (shunt model) and the potential drop due to the electrode's contact impedance z_l. The complete electrode model is then expressed as (1) together with boundary conditions (3), (4) and

$$u + z_l \sigma \frac{\partial u}{\partial \mathbf{n}} = V_l \quad \text{on} \ \ e_l, \quad l = 1, 2, \ldots, L \tag{5}$$

$$\sigma \frac{\partial u}{\partial \mathbf{n}} = 0 \quad \text{in the gaps between electrodes.} \tag{6}$$

To ensure a unique solution, the conservation of charge theorem must also hold, together with a choice of a reference voltage

$$\sum_{l=1}^{L} I_l = 0 \quad \text{and} \quad \sum_{l=1}^{L} V_l = 0. $$

B. Numerical Approximation and Forward Solution

A technique often used to solve the system of partial differential equations (1–6) is the finite element method (FEM) [107], [108]. This technique is based on transforming the continuous form of the problem into a discrete approximation constructed as a finite collection of K elements with constant conductivity, interconnected through N nodes (Fig. 3). Considering that during the fabrication of an artificial sensitive skin a thin material (or layers of thin materials) is used, only the two-dimensional surface EIT problem is commonly considered; interpolation can be used, however, to project the elements of the two-dimensional FEM to a three-dimensional space [109]. Then, applying FEM theory [109], [110] and rearranging the discretized system of equations leads to

$$\mathbf{Y} = \mathbf{Q}\mathbf{A}^{-1} \tag{7}$$

where $\mathbf{Y}$ is a vector of potentials at the N finite element nodes, $\mathbf{Q}$ is a set of current injection patterns at the electrodes, and $\mathbf{A}$ is known as the symmetric admittance matrix. This matrix associates each of the K elements with its constituent nodes and its conductivity.

Given the discrete FEM approximation for a known conductivity distribution within the domain, and a current injection pattern, the resulting boundary potentials can be calculated as the solution to the forward problem which—in contrast to the inverse problem—is well-posed and has a unique solution. For the small two-dimensional problems encountered in the case of an artificial sensitive skin, standard approaches to solving the linear system can be used; for example QR factorisation [112], LU factorisation or Cholesky factorisations [113]. Direct solution of large three-dimensional EIT systems can be computationally expensive and iterative methods such as conjugate gradient [14], preconditioned conjugate gradient [114] and algebraic multigrid preconditioned conjugate gradient [115] should be used.

C. Inverse Solution and Image Reconstruction

The EIT reconstruction problem is to find the internal conductivity distribution of an electrically conductive domain when a set of injected currents and the resulting boundary potentials are known. This is an ill-posed non-linear inverse problem in which the main complications are that the reconstructed image is not necessarily a unique solution and small changes in the boundary data can result in large unpredictable changes in the reconstructed image.

A number of methods exist for EIT inverse solution and image reconstruction. To some extent, they all follow the same basic approach: if the problem is non-linear, then linearise it; if the problem is ill-posed, then use regularisation to find a nearby well-posed problem; if the linear approximation is not accurate, then approach the solution iteratively. In principle these methods are divided into two groups: static imaging and dynamic imaging.

In *static imaging* [116] the absolute values of the conductivity distribution inside the domain are reconstructed, commonly in a "slow" iterative manner. *Dynamic imaging* [94] or *difference imaging*, on the other hand, is a fast one-step (non-iterative) method that reconstructs only the dynamic time-varying distribution of conductivity changes. Although the reconstruction of conductivities based on static imaging methods has the potential to be more accurate, for the robotics applications presented in this review only the conductivity changes are required and the ability to perform reconstructions in real time is a high priority. Dynamic imaging is therefore commonly used in applications that require real-time image reconstruction.

The essence of dynamic imaging is to first calculate the initial set of potentials $\mathbf{V}$ on the boundary of an assumed homogenous domain with "known" conductivity $\boldsymbol{\sigma}_0$. The discrete model is then replaced by a linear approximation that is used to compute only the conductivity difference $\delta\boldsymbol{\sigma}$ from the homogeneous case. Then, after calculating the Jacobian $\mathbf{J}$ between changes in boundary potential and internal conductivity, the discrete form of the linearised problem becomes

$$\delta\mathbf{V} \approx \mathbf{J}\delta\boldsymbol{\sigma} + \mathbf{w}, \qquad (8)$$

where $\delta\mathbf{V} = \mathbf{V}_2 - \mathbf{V}_1$ is the difference in potential between two measurements and $\mathbf{w}$ is a vector of measurement noise. The time-varying distribution of conductivity changes can be evaluated by taking two different sets of potential measurements ($\mathbf{V}_1$ and $\mathbf{V}_2$) at two different times (t_1 and t_2) and computing the difference $\delta\boldsymbol{\sigma}$ from $\delta\mathbf{V}$. Since only conductivity changes are calculated this method is fast and also reduces possible problems with unknown contact impedance and inaccurate electrode positions. Due to its robustness in computing conductivity changes, this method is often used in combination with a point-electrode model in which electrodes are considered to be single nodes in the mesh, and contact impedance between the electrode and the conductive domain is ignored [17]. The complete electrode method, however, will give improved accuracy of the reconstructions with negligible increase in computational cost.

1) Jacobian Calculation: The Jacobian $\mathbf{J}$ or *sensitivity matrix* is the derivative with respect to conductivity of the non-linear function that maps perturbations in the internal conductivity of the domain to changes of potential on the boundary. The Jacobian can be calculated numerically by perturbing the conductivity of each of the K elements in the FEM mesh by $\delta\boldsymbol{\sigma}$, and then solving the forward problem (7) to calculate the changes of potential $\delta\mathbf{V}$ at the electrodes. A difference approximation for $\mathbf{J}$ is obtained by dividing $\delta\mathbf{V}$ by $\delta\boldsymbol{\sigma}$ to give the Jacobian

$$J_{i,j} \approx \frac{\partial V_i}{\partial \sigma_j}; \quad i = 1 \dots M; \quad j = 1 \dots K,$$

where M is the number of potential measurements on the boundary. A direct calculation is computationally expensive and is therefore not recommended for large three-dimensional domains. The reader is referred to [101], [102], and [117] for alternative approaches suitable for the three-dimensional case.

Since little current passes through most of the elements, many entries in the Jacobian matrix will have values close to zero. Dividing by such small values causes numerical sensitivity in the solution so that small changes in measured potentials, such as those due to electrical noise, can cause large changes in the reconstruction; this ill-conditioned problem has to be solved by regularisation.

2) Regularisation: Informally, regularisation means that additional (prior) information is introduced so that an ill-posed problem—such as recovering the internal conductivity changes given the potentials on the boundary (8)—can be replaced by a nearby well-posed problem. Regularisation involves a trade-off between the "exact" but unstable solution based on the measured data, and a more stable "approximate" solution controlled by an imposed prior. In EIT-based artificial skin the additional information is usually an assumption that the spatial distribution of $\delta\boldsymbol{\sigma}$ is smooth; see Fig. 13 for an example.

Conventional regularisation methods include Tikhonov regularisation and approaches based on the singular value decomposition (SVD) [14], [100]. Although SVD is an important tool for understanding the ill-conditioning of matrices,

Tikhonov regularisation is more commonly accepted because its computation is simpler and more efficient.

The essence of the generalised Tikhonov regularisation is to solve the ill-conditioned problem

$$\delta\boldsymbol{\sigma} = \mathbf{J}^{-1}\delta\mathbf{V}$$

through minimisation of the least-square function

$$\min_{\delta\boldsymbol{\sigma}} \left\{ \|\mathbf{J}\delta\boldsymbol{\sigma} - \delta\mathbf{V}\|_2^2 + \alpha^2 \|\mathbf{R}(\boldsymbol{\sigma}_0 - \boldsymbol{\sigma}_r)\|_2^2 \right\}, \qquad (9)$$

where α is a scalar hyperparameter that controls the amount of regularisation, $\mathbf{R}$ is a regularisation matrix that controls the "smoothness" of the solution and $\boldsymbol{\sigma}_r$ is the initial reference conductivity, which is not necessarily the same as $\boldsymbol{\sigma}_0$.

Here, the trade-off is achieving a solution $\delta\boldsymbol{\sigma} = \mathbf{J}^{-1}\delta\mathbf{V}$ without $\delta\boldsymbol{\sigma}$ becoming unstable. As $\alpha \to 0$ the solution for $\delta\boldsymbol{\sigma}$ tends to the generalised (ill-conditioned) solution $\mathbf{J}^{-1}\delta\mathbf{V}$, while large amounts of regularisation (large α) tend to ignore the solution. For a regularisation matrix $\mathbf{R} = \mathbf{I}$, where $\mathbf{I}$ is the identity matrix, the penalty term $\alpha^2 \|\mathbf{R}(\boldsymbol{\sigma}_0 - \boldsymbol{\sigma}_r)\|_2^2$ in (9) prevents extreme values of conductivity $\boldsymbol{\sigma}$ but does not enforce any constraints on the solution. The formal solution to the problem (9), as given by Lionheart et al. [14], is

$$\delta\boldsymbol{\sigma} = (\mathbf{J}^{\mathrm{T}}\mathbf{J} + \alpha^2\mathbf{Q})^{-1}(\mathbf{J}^{\mathrm{T}}\delta\mathbf{V} + \alpha^2\mathbf{Q}(\boldsymbol{\sigma}_r - \boldsymbol{\sigma}_0)), \qquad (10)$$

where $\mathbf{Q} = \mathbf{R}^{\mathrm{T}}\mathbf{R}$. In addition, since in dynamic imaging only the changes in conductivity are measured, it can also be assumed that $\boldsymbol{\sigma}_r = \boldsymbol{\sigma}_0$. Then, for a fixed initial conductivity $\boldsymbol{\sigma}_0$, the Jacobian $\mathbf{J}$ and $(\mathbf{J}^{\mathrm{T}}\mathbf{J} + \alpha^2\mathbf{Q})^{-1}\mathbf{J}^{\mathrm{T}}$ can be pre-calculated off-line, greatly speeding up the solution.

3) Selection of a Regularisation Prior: In EIT imaging applied to artificial sensitive skin, it is commonly assumed that the conductivity of each element of the FEM mesh is constant and the spatial conductivity distribution is smooth (nearby elements have similar conductivity values) and a smoothing prior is therefore appropriate as the regularisation matrix $\mathbf{R}$. Naturally, if the real distribution of conductivity inside the domain is not smooth, then a different assumption for $\mathbf{R}$ should be used. Three different regularisation methods are commonly used [17].

a) Gaussian-type prior [94], [118]: A smoothing filter created by evaluating the regularisation matrix $\mathbf{R}$ as a discrete invariant Gaussian high-pass spatial filter. This approach penalises components with high spatial frequency in the reconstructed image by assuming higher correlation between neighbouring elements and a gradually diminishing correlation with increased distance. According to [110], in two-dimensional EIT the best performance can be obtained by using a Gaussian-type prior with a cut-off frequency selected so the spatial period is 10% the domain's length (or diameter).

b) Laplacian-type prior [94]: A smoothing approach that uses a discrete approximation of the Laplacian edge filter. This is a second-order filter that models inter-element correlations, penalises high spatial frequencies (edges), and smooths the solution.
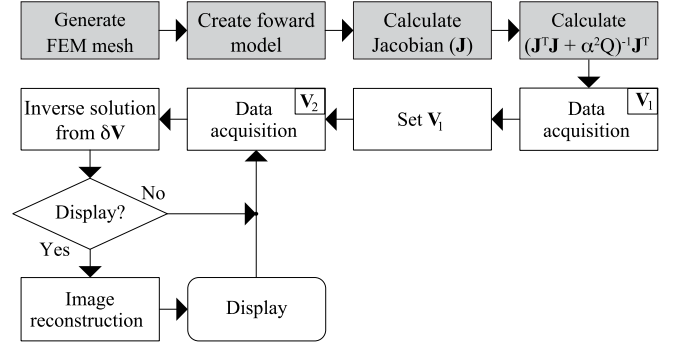

Fig. 4. Flow chart of experimental EIT. Grey shaded boxes in the figure represent off-line calculations.

c) Newton's one-step error reconstructor prior [119]: This algorithm utilises the first step of the Newton-Raphson method for non-linear equations with assumed homogeneous conductivity. When combined with the Tikhonov regularisation, it can be seen as a smoothing approach in which the regularisation matrix is scaled by the sensitivity of each element

$$\mathbf{Q} = diag\left[\mathbf{J}^T\mathbf{J}\right]^p,$$

where $p \in [0, 1]$.

4) Hyperparameter Selection: The hyperparameter α in (9) controls the trade-off between the solution based on measured data and an imposed prior controlled by the regularisation matrix. Correct selection of this parameter is crucial to achieving accurate reconstruction. A number of selection algorithms—such as the L-curve, generalised cross validation and fixed noise figure—exist in the field of inverse problems, but in EIT heuristic selection is still very common.

Comparisons between different regularisation algorithms can be subjective, complicated and inconsistent if heuristic methods are used. The above-mentioned methods were compared in Graham and Adler [118], where a new method of hyperparameter selection was introduced: the "BestRes" method. This method was shown to consistently produce a "good" reconstruction which in principle is similar to the "best" heuristic choice. A similar method, using resolution and error curves, was proposed by Silvera Tawil et al. [17]. This method, which allows for the comparison of several regularisation matrices in addition to hyperparameter values, was primarily implemented for EIT-based artificial skin applications.

5) On-Line Solution and Image Reconstruction: Once the forward model is created, all the parameters for inverse solution in (10) can be computed off-line from an assumed homogeneous conductivity distribution, as shown in Fig. 4. For difference imaging, two sets of potentials $\mathbf{V}_1$ and $\mathbf{V}_2$ are obtained at different times. The difference in potentials $\delta\mathbf{V}$ is then used to calculate the changes in conductivity $\delta\boldsymbol{\sigma}$ inside the domain. The inverse solution is computed inside a continuous loop that constantly updates both $\mathbf{V}_2$ and the inverse solution. Within the same loop $\delta\boldsymbol{\sigma}$ can be reorganised to display a two-dimensional representation (or three-dimensional interpolation) of conductivity changes based on the FEM model.

To simplify prototyping and development of EIT systems, the numerical implementation of the forward and inverse problems, together with image reconstruction, can be achieved using the EIDORS (electrical impedance tomography and diffuse optical tomography reconstruction software) project [120]. EIDORS is an open source software suite for image reconstruction in electrical impedance tomography and diffuse optical tomography, designed to facilitate collaboration, testing and new research in these fields.

IV. EIT-BASED SKIN FABRICATION

The main component of an EIT-based artificial skin is the variable-conductivity material used for its fabrication. An ideal material would be light-weight, low-cost, have continuous and homogeneous conductivity, give large, linear and local changes in conductivity in response to external stimulus (i.e. touch and pressure), have no hysteresis and no conductivity change as a result of flexing, stretching or changes in temperature or humidity.

A number of materials have been investigated with the aim of finding one that satisfies these criteria. The first EIT-based sensitive skin was created using a rubber mixed with conductive carbon particles to develop a flexible, single-layered, pressure-sensitive skin [15]. Due to the characteristics of the rubber, this skin was flexible but not stretchable. It also had high hysteresis and gave only small conductivity changes in response to pressure.

Conductive fabrics were investigated by Nagakubo et al. [16] who creating a highly-stretchable fabric by spraying a conductive water-based carbonic paint over the surface of an ordinary knit fabric. The surface conductivity of the material changed as it was stretched in-plane or compressed normal to the plane of the fabric. These changes were due to changes in the area of contact between the conductive yarns in the structure of the fabric. The conductive knit was not only more stretchable than the conductive rubber used in [15], but also had less hysteresis. Large conductivity changes due to stretch were, however, a significant disadvantage. The efficiency of this material was demonstrated by placing the artificial skin over flat and three-dimensional surfaces; see Fig. 5.

A similar approach, again using single-layered fabrics, was reported by Yao et al. [76], [80]. In [76], Yao and Soleimani used a highly conductive ($\sigma \approx 1000$ mS/sq) medical-grade silver-plated Nylon Dorlastan fabric, from Less EMF Inc., with the ability to stretch in both directions (Fig. 6(a)). As in [16], the surface conductivity of this material changes as it is stretched in-plane or compressed normal to the plane of the fabric. Furthermore, in [80] the authors used a non-woven microfibre conductive ($\sigma \approx 0.667$ mS/sq) fabric from Eeonyx Corp. (Fig. 6(b)). The reduced stretchability of this fabric reduces potential hysteresis effects, since no large-scale deformation can occur when pressure is applied.

To improve the response to pressure and to minimise changes in conductivity due to stretch, Silvera-Tawil et al. [121] used two layers of different fabrics instead of one. The bottom layer was a carbon-loaded conductive fabric from Eeonyx Corp. The surface conductivity ($\sigma \approx 12.5$ mS/sq) of this

(a) Stretchable artificial skin.   (b) Points of pressure.

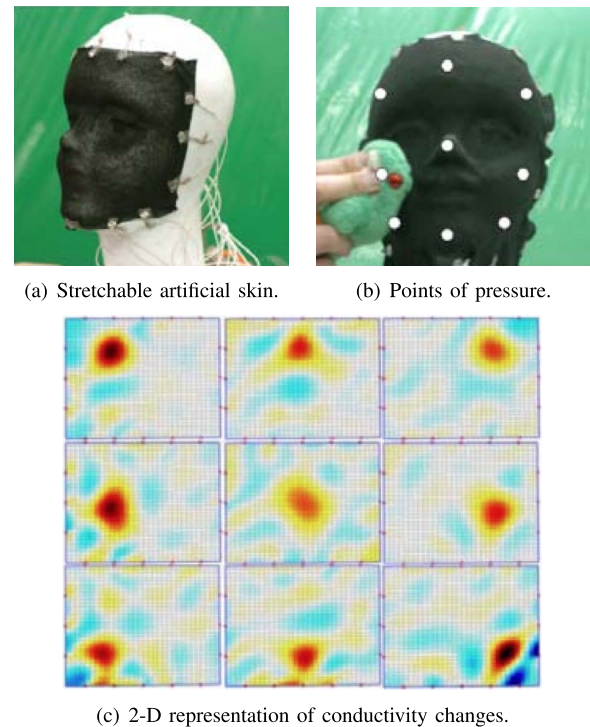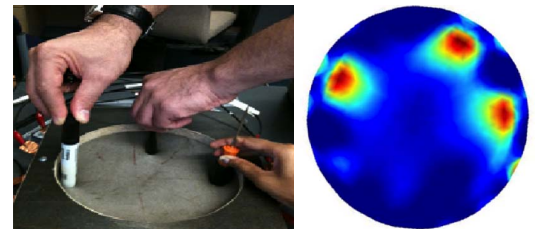(c) 2-D representation of conductivity changes.

Fig. 5. Highly stretchable single-layered EIT-based artificial skin. (a) Square of artificial skin placed over a complex three-dimensional surface. (b) Pressure applied over the artificial skin. (c) Two-dimensional representation of the reconstructed conductivity changes due to pressure applied at the locations represented by the white circles in (b). Figures reproduced from [16].

(a) Highly-stretchable single-layered EIT-based skin.
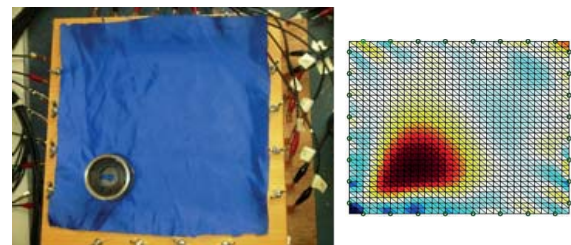
(b) Single-layered EIT-based skin with reduced stretchability.

Fig. 6. Single-layered EIT-based artificial skin. (a) Circular sensor manufactured using a highly stretchable conductive fabric (left) and two-dimensional representation of the reconstructed conductivity changes due to multiple points of pressure/stretch (right). (b) Squared sensor manufactured using a microfibre non-woven fabric (left) and two-dimensional representation of the reconstructed conductivity changes due to pressure (right). Figures adapted and reproduced from [76] and [80] with the author's permission.

material changes as it is stretched (maximum stretch $\approx 60\%$ in length and $\approx 35\%$ in width). Measuring electrodes were fixed to this layer. A second layer of thin, stretchable, highly conductive ($\sigma \approx 660$ mS/sq) silver-plated fabric (Less EMF Inc.)

(a) Exploded three-dimensional model.

(b) Finished artificial skin.   (c) 2D pressure reconstruction.
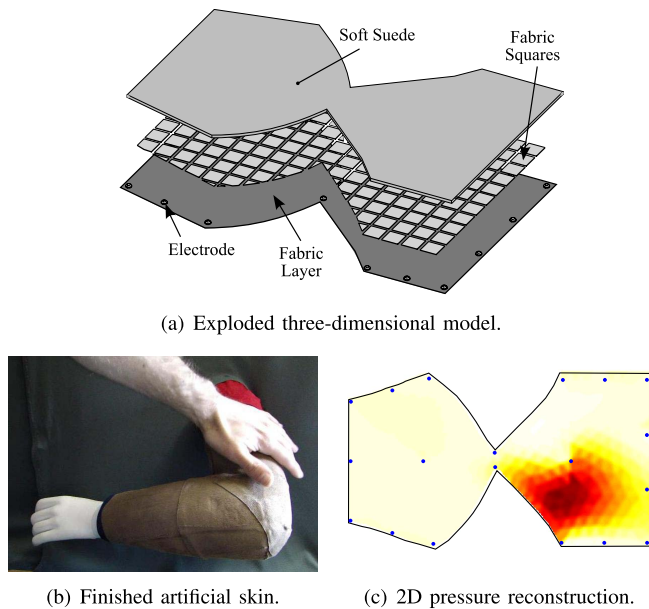
Fig. 7.   Multi-layered fabric-based artificial skin. Three-dimensional model of the irregularly shaped artificial skin (a), artificial skin placed over the surface of a three-dimensional artificial arm (b) and two-dimensional representation of the reconstructed conductivity changes due to pressure applied to the artificial arm (c). Figures reproduced and adapted from [110] with the author's permission.

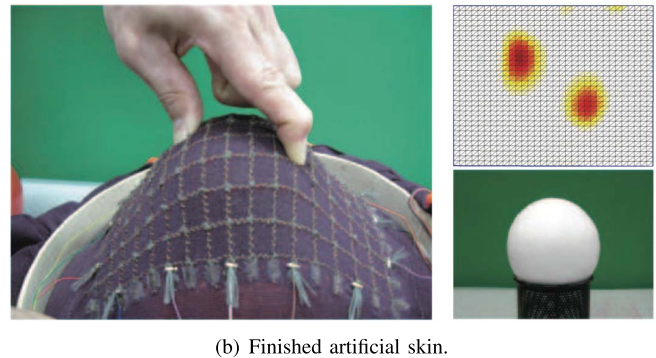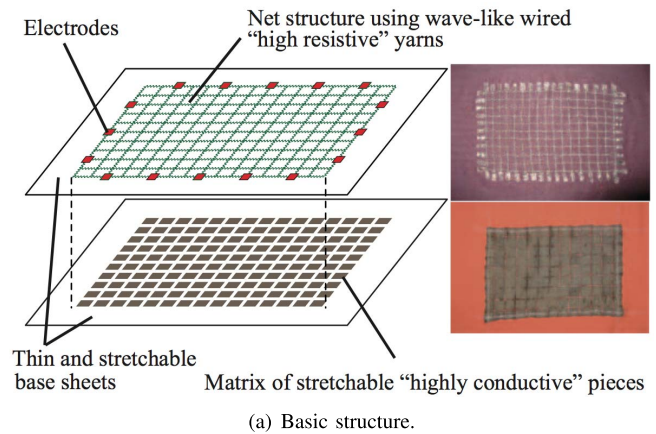(a) Basic structure.

(b) Finished artificial skin.

Fig. 8.   Multi-layered fabric and yarn-based artificial skin (a) Basic structure of the tactile sensor (left) and photos of the two layers before integration (right). (b) Developed tactile sensor under 2-way stretch (left) and two-dimensional representation of the reconstructed conductivity changes due to pressure applied to the stretched sensor (right). Figures reproduced from [75].

was placed on top of the first layer. By applying the theory of area of contact between the two layers, it was possible to detect conductivity changes as a result of applied pressure while reducing conductivity changes in response to stretch. To allow the detection of multiple simultaneous points of pressure, the second layer was made of unconnected discrete squares of fabric. This reduced the risk of current flowing between different contact points via the highly conductive fabric. To provide a more natural-looking artificial skin with a "pleasant" feel to touch, a soft suede fabric was placed on top to cover the active skin, see Fig. 7.

Alirezaei et al. [75] used a similar approach to [121] with the only difference being that instead of using two layers of fabrics, the bottom layer was made of a net of conductive copper sulphide bonded nylon yarn. By using wavelike yarns the total length of the yarns remained constant when the fabric was stretched, completely eliminating changes in conductivity (Fig. 8). In both these approaches, conductivity varies non-linearly with pressure due to the non-linear changes in the area of contact between the two layers, and within/between yarn in the conductive fabrics. Both approaches were tested over flat and three-dimensional surfaces.

To provide a soft insulating surface, non-conductive materials have been used to cover artificial sensitive skins [75], [80], [82], [121]. Additionally, this layer serves to redistribute pressure over the surface of the skin around the point of pressure, generating smooth two-dimensional changes in conductivity.

A. EIT Data Collection

A typical EIT system consists of one or more current sources, a switching mechanism for generating current injection patterns and a data acquisition unit for potential

measurements. Low frequency AC signals are commonly used as this eliminates long-term polarisation effects in the electrodes and allows measurement of the capacitive and resistive components of the conductive domain. Unfortunately, this method also requires synchronous analogue detection circuits and low-pass filters or digital processing techniques that not only significantly complicate hardware design (and increase cost), but also consume more power and affect real-time sampling performance [122], all of which are disadvantageous for a robotics application.

Cilliers et al. [123] introduced a bidirectional DC current pulse excitation technique, in which the current to the driving electrode is kept constant during each half cycle. The driving current waveform is then a zero-mean square wave, and potential measurements can be taken during the "flat" parts of the cycle once static electromagnetic conditions have been achieved (Fig. 9). The hardware is simplified, given that the measurements can be treated as DC signals. In addition, this approach eliminates long-term polarisation effects at the electrodes.

For robotics applications, the use of DC current excitation is desirable because of its simple implementation in battery-powered mobile hardware. Although a bidirectional excitation approach is preferred, unidirectional DC current excitation has been used for artificial sensitive skins due to its simple implementation [16], [121], [124]. In addition, this
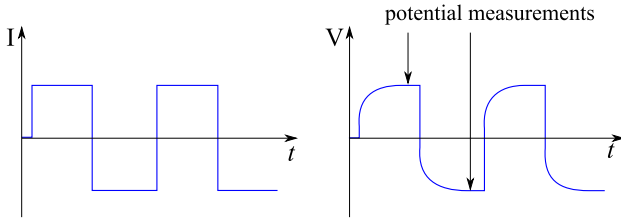
Fig. 9.   Theoretical form of bidirectional excitation pulses (left) and potential measurements (right). Potential measurements are taken after stationary electromagnetic conditions have been achieved.

Fig. 10.   First of sixteen steps for the adjacent drive pattern applied to a circular domain with sixteen boundary electrodes. In this step, current **I** is applied across a pair of adjacent electrodes (1 and 2) and the resulting potentials **V** are measured across all other adjacent electrodes. In the second step, current excitation is rotated to electrodes 2 and 3, and so on.

approach requires only a single data measurement at each cycle instead of the two required in the bidirectional method, thereby doubling sampling rates.

Many different strategies for current injection and potential measurement—henceforth termed "drive patterns"—can be applied in EIT. In general, they can be divided into two groups: optimal (multi-source) patterns and bipolar (single-source) patterns.

1) Optimal Patterns: Based on the concept of distinguishability [125], which states that ideal current patterns are obtained by maximising the difference between potential measurements at the boundary of the conductive domain resulting from two predetermined conductivity distributions [126], [127]. Optimal patterns require multiple current sources that are simultaneously used for current injection while potential measurements are taken at all boundary electrodes. In Hua et al. [128], for example, $L - 1$ independent current injection patterns are applied to the electrodes while potentials are measured at all L electrodes.

It has been argued that the optimal current pattern that best distinguishes a central circular inhomogeneity inside a circular homogenous domain is the *trigonometric* current pattern [129], [130]. Cheney and Isaacson [131], however, demonstrated that if the power consumption during electrode excitation is kept fixed at a predefined value, the polar pattern will result in even better distinguishability of a centred target.

Even if optimal patterns have the potential to produce very accurate image reconstructions, they also need as many independent AC current sources as there are electrodes. This is not practical for a robotics application.

2) Bipolar Patterns: Bipolar patterns are those in which a single current source and sink are used to inject current through a single pair of electrodes at a time, while potential measurements are taken at all remaining electrodes pairs. The bipolar drive pattern that is most commonly used is termed the *adjacent* [93], [98], [132] or *neighbouring* [100] method. In this method current is injected through a pair of adjacent electrodes while the resulting potentials are measured at all other adjacent electrode pairs, Fig 10. The current injection pair is then systematically rotated through all adjacent electrode pairs while potential measurements are taken from all remaining adjacent electrode pairs. To achieve a constant dynamic range in the data, potential measurements are typically not made at electrodes carrying injected current.

Since this method is symmetrical—there is complete and symmetrical interchange of current injection and potential measurement—the reciprocity principle [133] holds.
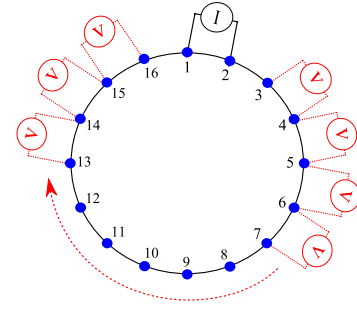
Accordingly, for the adjacent method using sixteen electrodes a total of 104 independent potential measurements are available. That is,

$$\text{Total\_Measurements} = \frac{L(L-3)}{2}, \qquad (11)$$

where L is the total number of electrodes on the boundary.

Several bipolar drive patterns have previously been compared [17], [77], [98], [134], [135] with the aim of finding a pattern that provides the best resolution and performance in the presence of noise. It has been argued [134] that the best spatial resolution can be obtained by using an adjacent pattern. This pattern, unfortunately, also provides the worse performance in the presence of noise [134], [135], particularly in the centre of the conductive domain where current flow is, on average, the least.

Although the current injected into the domain could be increased to improve signal-to-noise ratio (SNR), in a battery-driven application the system is limited in power so that increasing current flow is not a practical solution. Increasing the number of boundary electrodes would provide more potential measurements which, at the same time, would yield more information about the internal conductivity distribution—particularly near the boundary. Unfortunately, it would also compromise the real-time efficiency of data acquisition required for a robotics application.

An improved approach is to utilise a drive pattern that better distributes current density across the conductive domain. Shi et al. [98] observed that the best performance was achieved with a pseudo-polar pattern in which the current sink electrode is located exactly one electrode before the electrode opposite to the source. The reason for the performance improvement is that injecting current through electrodes that are almost opposite increases the current density right across the conductive domain, thus improving resolution in the centre of the domain. The potentials at the boundary electrodes also increase, thus improving SNR in the presence of the same amount of noise. In addition, by removing symmetry between current injection and potential measurement patterns (i.e. removing reciprocity), all measurements are independent and more information about the internal conductivity distribution is obtained.

Although the polar pattern, in which the current source and sink are 180° apart, shares some of the advantages (improved current density and SNR) of the pseudo-polar pattern, its

symmetry halves the number of independent measurements, resulting in a great loss of internal conductivity information.

Given that a thin layer (or layers) of conductive material is used to fabricate an artificial skin, another means of improving performance is to add electrodes in different locations *within* the conducting domain [17]. Such a configuration provides additional improvements in both resolution and robustness to noise in the reconstructed image. The best improvements can be attained by adding electrodes in locations where the worst performance—due to low current flow—is otherwise expected. Since the cited work [17] uses internal electrodes only as references for potential measurement or current injection, the real-time performance of the system is not sacrificed. As there is a complete absence of conductivity changes at the electrode locations, small internal electrodes are highly recommended. Note that the mathematical model presented in Sec. III only considers electrodes attached at the boundary of the domain. Heikkinen et al. [136], however, present a model that allows for internal electrodes to be incorporated by assuming that the FEM model in Sec. III-B is changed from the conventional approach with a single external boundary to an approach that includes internal and external boundaries. Electrodes are thereby not strictly placed within the conductive domain, but on the inner boundaries of the domain. When these assumptions are made, the same mathematical model and boundary conditions presented previously can be applied.

B. Hardware Implementation

The electronic hardware for an EIT-based artificial skin for robotics applications should satisfy the requirements defined in previous sections. These can be summarised as:

1) Bipolar current patterns are preferred over optimal patterns to simplify hardware implementation.
2) For a battery-driven application, DC current sources are preferred. Potential measurements should be taken after static electromagnetic conditions have been achieved.
3) Internal electrodes can be used as references for potential measurements to improve image reconstruction without sacrificing real-time performance of the system.
4) To achieve a constant dynamic range in the data, potential measurements from electrodes carrying injected current are not acquired.

A variety of different approaches can be used to achieve these requirements, but in general all hardware follows the same configuration. A single current source is time-multiplexed across multiple current injection channels. At any time step, two channels are selected as current source and current sink, and potential measurements are taken from all remaining channels by multiplexing one or more voltage acquisition channels. In Fig. 11, for example, a current source is multiplexed through 16 boundary electrodes of a circular conductive domain. A microprocessor is used to control and synchronise both current injection and potential measurement patterns. Data acquisition from all channels is handled by the potential measurement multiplexer.

The number of electrodes used in an implementation should be chosen as a compromise between the spatial resolution and
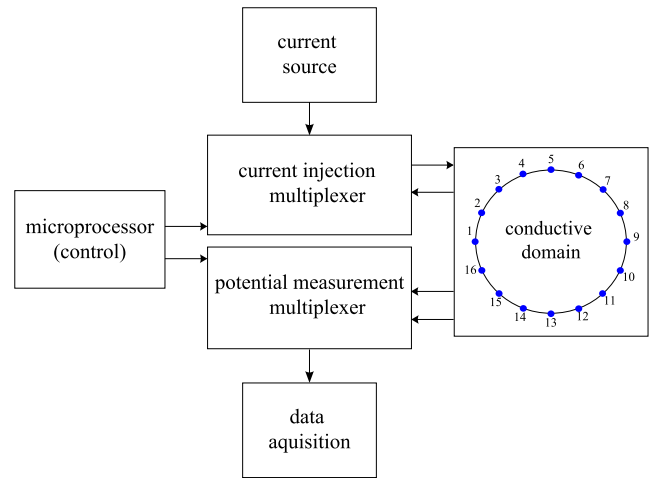

Fig. 11.   Block diagram of generic EIT hardware.

the real-time reconstruction rate required for an application. Increasing the size of the skin without increasing the number of electrodes will cause a reduction in the spatial resolution. A total of 104 independent measurements are available from sixteen boundary electrodes using the adjacent pattern. These measurements result in a spatial resolution of approximately 10% of the characteristic dimension of the conductive domain ($1/\sqrt{104} \approx 10\%$). Increasing the number of boundary electrodes to 24, for example, would provide 252 independent measurements giving an improvement in resolution of approximately 3.5% ($1/\sqrt{252} \approx 6.5\%$). The sampling time would be strongly affected, however, since more than double the number of measurements are required.

The image reconstruction bandwidth of an EIT-based system is the rate at which the continuous loop in Fig. 4 can be executed. This rate depends on the time required to acquire a complete cycle of electrode potentials and then compute the inverse solution. The complexity of the inverse solution varies linearly with the number of elements in the Jacobian (10). Approximate reconstruction rates of 45 Hz were reported in [82] and [110] for systems with up to 17 boundary electrodes. In this case, data were acquired using LabVIEW and an ADLINK Technology Inc. board to sample at approximately 1.8 kHz per channel, while inverse solution and image reconstruction were implemented in MATLAB. A similar approach was followed in [76]. Alirezaei et al. [124], on the other hand, reported sampling and communication rates of up to 30 Hz using an Analog Devices ADS1258 converter ($\approx$23 kHz) over a microcontroller running ART-Linux. Unfortunately, image reconstruction rates were not reported.

The power consumption of an EIT system depends on the losses within the resistive skin and on the electronics hardware for data acquisition and computation. All bipolar EIT drive patterns have only one current source active at any time. The current must be sufficiently high to raise the voltage changes at electrodes above the noise floor for a particular touch sensitivity. The base resistivity of the EIT material should therefore be relatively high to minimise power consumption. Silvera-Tawil [110] reported a resistive power loss of

approximately 22 mW (1.8 mA at 12 V) while Yao and Soleimani [76] reported approximately 175 mW (10 mA through 1 Ohm/sq at a frequency of 2 kHz).

Although these performance figures are from early experimental implementations of real-time EIT-based sensitive skin systems, it is clear that real-time implementations with pressure sensing bandwidths of 45 Hz or more are within the capabilities of current technology. Advances in field-programmable logic device and application-specific integrated circuit technology, including the integration of "soft" microprocessors, are likely to lead to further increases in performance.

At this early stage of their development there is no information available on the robustness and reliability of EIT-based sensitive skins. As with power consumption and performance figures, the reliability of the electronics and computational components depends strongly on the quality of their design and implementation. Robustness in service depends critically on mechanical properties of the EIT material such as toughness, resilience and flexibility, and on the electrically and mechanically robust attachment of electrodes to the material. Additional work is necessary to develop highly robust variable-resistance materials that are flexible and stretchable while maintaining long-term electrical stability.

V. Skin Evaluation and Performance Metrics

Assessing the quality of a reconstructed image in EIT is difficult. Reconstructed images are only approximate representations of the internal conductivity distribution, and their accuracy depends strongly on the reconstruction algorithm and its parameters. Several metrics have been used—see [94], [110], [137], [138]—in attempts to find a set that objectively measures the "quality" of a reconstructed image. Metrics analogous to those used when evaluating the human sense of touch were suggested in [110] to evaluate a sensitive skin. In general, performance metrics for EIT-based artificial skin applications can be summarised as follows:

A. Spatial Resolution (RES)

Based on the "two point discrimination threshold" that measures the ability of a person to discriminate between two simultaneous stimuli [11], this metric evaluates a ratio between the area of the conductive domain and the area of the reconstructed image containing at least 50% of the maximum amplitude. As the spatial resolution increases, so does the capability of the system to discriminate between two different stimuli rather than to mis-reconstruct them as one. In [137] and [138] areas were approximated by using the number of image pixels, while in [110] the averaged size of the FEM elements was considered. In both cases the square root of the ratio was used to measure length ratios rather than area ratios.

The relatively low spatial resolution of EIT-based skin, as compared with other tactile sensing technologies [21], [27], and a poor ability to discriminate between pressure intensities and contact areas also affects its capacity to discriminate between stimuli and makes it unsuitable for applications where high spatial resolution is required. Spatial resolution
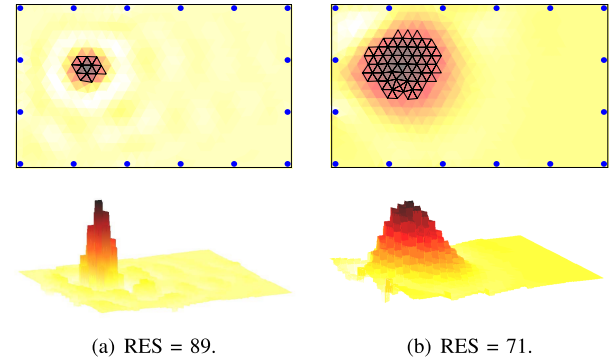

(a) RES = 89. (b) RES = 71.

Fig. 12. Images of two different reconstructions of conductivity changes due to a (simulated) stimulus on a rectangular conductive domain with sixteen boundary electrodes. Image (a) is the best in terms of RES computed by FEM element, as proposed in [110]. Black bordered triangles in the two-dimensional representation are the FEM elements above the 50% maximum amplitude, and considered for the calculation.
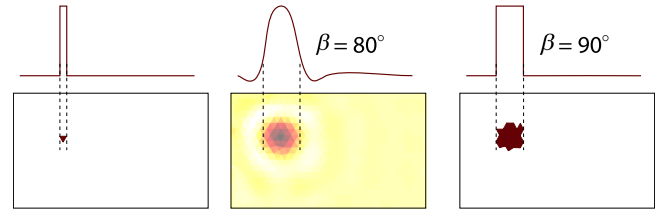

Fig. 13. Illustration of different reconstructed images due to a simulated stimulus (left): smooth reconstruction (centre) and discontinuous reconstruction (right). The bottom row shows the image while the top row plots a lateral slice of the reconstruction.

varies depending on drive pattern, regularisation algorithm and number and location of electrodes. Higher pressures mask nearby lower pressures, and it is more difficult to discriminate when two touches occur at the same time. See Fig. 12 for an example of a stimulus reconstructed at two different spatial resolutions.

B. Shape Deformation (β)

The "shape" of the reconstructed image can be assessed by using the difference between its spatial resolutions calculated at 50% and 75% of the maximum amplitude, as proposed in [110]. For a discontinuous reconstruction, the spatial resolution at the 50% and 75% maximum amplitudes is expected to be the same, as shown in Fig. 13. This metric is similar to the *shape deformation* metric proposed by Adler et al. [138] in which the difference between two assumed circular areas is computed. In this case, however, a more generalised metric is obtained by removing the assumption of "circular" reconstructions and computing the absolute differences instead.

C. Position Error (PE)

Inspired by the "point localisation" metric which evaluates the capacity of a person to locate the position of a tactile stimulus [11], this metric computes the distance between the centroid of the stimulus (x_1, y_1) and the centroid of the reconstructed image (x_2, y_2), see Fig. 14. In [110],
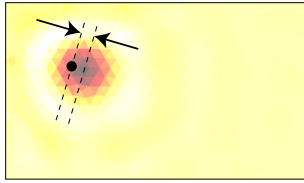
Fig. 14. Illustration of a reconstruction pushed to the centre of the conductive domain (positive PE). The small solid (black) circle marks the real location of the stimulus.

Silvera-Tawil et al. used the Euclidean distance to represent absolute position errors, while a more generalised approach was proposed by Adler et al. [138] who considered both magnitude and direction. As a result, negative values of PE indicate reconstructed images being "pushed" closer to the boundaries of the conductive domain while positive values of PE indicate reconstructed images "pushed" to the centre.

In both cases ([110] and [138]), a position error of zero (PE = 0), with no variability for stimulus at different locations would represent perfect performance by this measure. Similar to the spatial resolution metric, in EIT position error accuracy varies depending on the drive pattern, reconstruction algorithm, total number and location of electrodes.

D. Amplitude Response

This metric measures the ratio of image amplitudes in the stimulus, represented by pixels, to that in the reconstructed image. As described by Adler et al. [138], the desired behaviour is to achieve constant intensity change due to the same stimulus at any position across the conductive domain. In EIT-based skins amplitude response is not linear with applied pressure. This is due to the non-linearity of EIT as a function of touch location, the effects of the area of contact on changes in the conductivity distribution, and the characteristics of the materials used for skin fabrication.

E. Temporal Information

Temporal information refers to the ability of the system to identify changes in the touch stimulus applied to the skin over the time of contact. For an artificial skin designed for HRI, for example, a minimum update frequency of 20 Hz is desired (Sec II).

VI. Touch Interpretation

The interpretation of touch in robotics and, in particular, via a sensitive skin is a vast, unresolved research area that will play a crucial role in the further development of robotics. Due to their limitations (Sec. II), EIT-based artificial skins are not suitable for applications such as grasping, fine manipulation and texture recognition and have typically been used in touch recognition for human-robot interaction.

In this vein, Alirezaei et al. [75] demonstrated the possibilities of using a stretchable EIT-based sensitive skin placed over a three-dimensional surface to detect tactile gestures such as pinching, pushing and rubbing. The skin used during these experiments was manufactured by the authors of [75] using a net of yarn over a highly stretchable knit fabric of rectangular shape (90 mm × 160 mm) with 16 boundary electrodes; see Fig. 5. Data were acquired using an adjacent sampling method at a maximum image reconstruction rate of 40 Hz. Tactile gestures were displayed on a computer screen and detected visually.

Silvera-Tawil et al. [82], [84] used machine learning algorithms to classify autonomously nine different tactile gestures [82] and twelve discrete emotions and social messages [84] commonly transmitted by humans via touch. Human touch was conveyed to a full-sized three-dimensional mannequin arm covered with an irregularly shaped (≈490 mm × 274 mm) EIT-based artificial skin, see Fig 7. The artificial skin was manufactured using two layers of highly stretchable conductive fabric with 16 boundary electrodes and two internal electrodes. Data was acquired using a 'RefTwo' bipolar pattern [17], which considers two internal reference electrodes—in addition to boundary electrodes—during data acquisition. Touch classification was achieved using a LogitBoost algorithm and attributes of touch—such as pressure intensity, touch location and area of contact—extracted at approximately 40 Hz. Experimental results demonstrated that autonomous classification of social touch can be achieved at better-than-chance levels, using an EIT-based artificial skin, and with accuracies comparable to those achieved by humans.

Although in all the cases mentioned above touch interpretation was performed from attributes of touch extracted from the two-dimensional reconstructed image, machine learning algorithms allow for data to be processed at two earlier stages: (1) just after data acquisition (raw data), as shown in Fig. 4, and (2) after inverse solution. By processing data at an earlier stage, the CPU time typically required for the mathematical calculation and image reconstruction can be reduced. Although the first approach (before inverse solution) would reduce data computation to a minimum the lack of prior information introduced through the regularisation process would make the interpretation step more complex.

VII. Discussion and Conclusion

This paper presented a review on EIT as the underlying technology for the creation of an artificial sensitive skin for robotics. The benefits of an EIT-based artificial skin are clear when it is conceptualised as a single piece of thin, stretchable and flexible material that could be cut into any shape and used to cover small and large areas of three-dimensional robotic structures. This skin, which has the ability to sense pressures due to touch in real time, can be driven by a small number of electrodes and associated wiring. All stages of sensing from data acquisition to the preprocessing of localised touch information can be controlled using the same hardware. Because a single piece of material is used, the calibration process is simple. That is, only one sensor element is calibrated without the need to account for the locations of multiple discrete sensors. As the only requirement of such a system

is that the material must change its local conductivity in response to external excitation, materials sensitive to physical phenomena other than pressure could also be used.

Developing an EIT-based skin is not an easy task. The characteristics of the material used to construct the skin play a significant role in its performance. Unfortunately, the "perfect" material—a material that would generate large, local changes in conductivity due to touch, would provide continuous, linear changes as a result of increased pressure, and would not change as a result of stretch—is not commercially available, and the latest approaches rely in incorporating multiple layers of different materials, such as conductive yarns and fabrics, that allow for artificial skin that are sensitive to pressure yet minimise the effects of stretch. These approaches, however, also suffer the disadvantages that exist in any sensor manufactured using conductive fabrics. These include complicated electrode connections, non-linear responses, susceptibility to electrical noise, degradation of response over time and high hysteresis. Future research is required to develop materials better suited to EIT-based skins, and to use these materials in combination with existing hardware and software.

When using EIT, the spatial resolution capabilities of the artificial skin can be adjusted quickly and easily by simply altering the number of boundary and internal electrodes that are used during image reconstruction. Regardless of the spatial resolution obtained, an EIT-based skin always functions as a continuous sensor. In terms of adaptability and scalability, EIT allows for the same manufacturing principle to be used to create artificial skins of different sizes and shapes and use them to cover flat and three-dimensional surfaces [75], [80], [82]. No noticeable changes in the characteristics of the skin have been reported as a result of its placement on a three-dimensional surface.

The spatial resolution of EIT-based skin is, however, low compared with other artificial skin technologies, and is strongly dependent on the size of the skin and the number of electrodes used. A compromise between the size of the skin, the number of boundary and internal electrodes (which affects the real-time efficiency of data acquisition) and the spatial resolution is needed.

Future work should consider new flexible and stretchable materials with linear electro-mechanical behaviour, an electro-mechanical forward model which considers the material's characteristics and new regularisation methods that incorporate more information about the material's conductivity changes in the material that would improve the quality of the reconstructed images and allow for better discrimination between area of contact and pressure intensity. Conductivity changes due to electrode movement as a result of the robot's behaviour should be taken into account [139]. In addition, significant work is required to integrate EIT-based artificial skins within a full-scale robotics application in which multiple robot body parts should be covered. In this case, a compromise between the size of the skin, number of electrodes and spatial resolution at different locations might be needed. Multiple pieces of the artificial skin could be used to cover different body parts.

REFERENCES

[1] M. A. Goodrich and A. C. Schultz, "Human-robot interaction: A survey," *Found. Trends Human-Comput. Interact.*, vol. 1, no. 3, pp. 203–275, 2007.
[2] C. Harper and G. Virk, "Towards the development of international safety standards for human robot interaction," *Int. J. Soc. Robot.*, vol. 2, no. 3, pp. 229–234, 2010.
[3] Z. Zeng, M. Pantic, G. Roisman, and T. Huang, "A survey of affect recognition methods: Audio, visual, and spontaneous expressions," *IEEE Trans. Pattern Anal. Mach. Intell.*, vol. 31, no. 1, pp. 39–58, Jan. 2009.
[4] V. J. Lumelsky, M. S. Shur, and S. Wagner, "Sensitive skin," *IEEE Sensors J.*, vol. 1, no. 1, pp. 41–51, Jun. 2001.
[5] J.-H. Kim, J.-I. Lee, H.-J. Lee, Y.-K. Park, M.-S. Kim, and D.-I. Kang, "Design of flexible tactile sensor based on three-component force and its fabrication," in *Proc. IEEE Int. Conf. Robot. Autom.*, Apr. 2005, pp. 2578–2581.
[6] K. Kim *et al.*, "A silicon-based flexible tactile sensor for ubiquitous robot companion applications," *J. Phys., Conf. Ser.*, vol. 34, no. 1, pp. 399–403, 2006.
[7] R. S. Dahiya, P. Mittendorfer, M. Valle, G. Cheng, and V. J. Lumelsky, "Directions toward effective utilization of tactile skin: A review," *IEEE Sensors J.*, vol. 13, no. 11, pp. 4121–4138, Nov. 2013. [Online]. Available: http://dx.doi.org/10.1109/JSEN.2013.2279056
[8] R. S. Dahiya, G. Metta, M. Valle, and G. Sandini, "Tactile sensing—From humans to humanoids," *IEEE Trans. Robot.*, vol. 26, no. 1, pp. 1–20, Feb. 2010.
[9] D. Silvera-Tawil, D. C. Rye, and M. Velonaki, "Artificial skin and tactile sensing for socially interactive robots: A review," *Robot. Auto. Syst.*, vol. 63, no. 3, pp. 230–243, 2015.
[10] P. Mittendorfer and G. Cheng, "Humanoid multimodal tactile-sensing modules," *IEEE Trans. Robot.*, vol. 27, no. 3, pp. 401–410, Jun. 2011.
[11] S. Lederman, "Skin and touch," in *Encyclopedia of Human Biology*, vol. 7, R. Dulbecco, Ed. New York, NY, USA: Academic, 1991, pp. 51–63.
[12] E. Weber, *On the Tactile Senses*, D. Murray, H. Ross, and E. Weber, Eds. New York, NY, USA: Academic, 1978.
[13] M. L. Hammock, A. Chortos, B. C.-K. Tee, J. B.-H. Tok, and Z. Bao, "25th anniversary article: The evolution of electronic skin (e-skin): A brief history, design considerations, and recent progress," *Adv. Mater.*, vol. 25, no. 42, pp. 5997–6038, 2013.
[14] W. Lionheart, N. Polydorides, and A. Borsic, "The reconstruction problem," in *Electrical Impedance Tomography: Methods, History and Applications*. London, U.K.: Inst. Physics Pub., 2005, ch. 1, pp. 3–64.
[15] Y. Kato, T. Mukai, T. Hayakawa, and T. Shibata, "Tactile sensor without wire and sensing element in the tactile region based on EIT method," in *Proc. IEEE Sensors*, Oct. 2007, pp. 792–795.
[16] A. Nagakubo, H. Alirezaei, and Y. Kuniyoshi, "A deformable and deformation sensitive tactile distribution sensor," in *Proc. IEEE Int. Conf. Robot. Biomimetics*, Dec. 2007, pp. 1301–1308.
[17] D. S. Tawil, D. Rye, and M. Velonaki, "Improved image reconstruction for an EIT-based sensitive skin with multiple internal electrodes," *IEEE Trans. Robot.*, vol. 27, no. 3, pp. 425–435, Jun. 2011.
[18] R. Lazzarini, R. Magni, and P. Dario, "A tactile array sensor layered in an artificial skin," in *Proc. IEEE/RSJ Int. Conf. Intell. Robots Syst.*, vol. 3, Aug. 1995, pp. 114–119.
[19] T. V. Papakostas, J. Lima, and M. Lowe, "A large area force sensor for smart skin applications," in *Proc. IEEE Sensors*, vol. 2. Jun. 2002, pp. 1620–1624.
[20] W. D. Stiehl and C. Breazeal, "A sensitive skin for robotic companions featuring temperature, force, and electric field sensors," in *Proc. IEEE/RSJ Int. Conf. Intell. Robots Syst.*, Oct. 2006, pp. 1952–1959.
[21] T. Someya, T. Sakurai, and T. Sekitani, "Large-area electronics based on organic transistors," in *Proc. 64th IEEE Device Res. Conf.*, Jun. 2006, pp. 209–210.
[22] W. D. Stiehl and C. Breazeal, "Applying a 'somatic alphabet' approach to inferring orientation, motion, and direction in clusters of force sensing resistors," in *Proc. IEEE/RSJ Int. Conf. Intell. Robots Syst.*, vol. 3, Sep./Oct. 2004, pp. 3015–3020.
[23] T. Lomas, A. Tuantranont, and A. Wisitsoraat, "Polysilicon piezoresistive tactile sensor array fabricated by polyMUMPs process," in *Proc. 5th IEEE Conf. Sensors*, Oct. 2006, pp. 1313–1316.
[24] T. Mukai, M. Onishi, T. Odashima, S. Hirano, and Z. Luo, "Development of the tactile sensor system of a human-interactive robot 'RI-MAN,'" *IEEE Trans. Robot.*, vol. 24, no. 2, pp. 505–512, Apr. 2008.

[25] J. Meyer, P. Lukowicz, and G. Tröster, "Textile pressure sensor for muscle activity and motion detection," in *Proc. IEEE Int. Symp. Wearable Comput.*, Oct. 2006, pp. 69–72.

[26] G. Cannata, M. Maggiali, G. Metta, and G. Sandini, "An embedded artificial skin for humanoid robots," in *Proc. IEEE Int. Conf. Multisensor Fusion Integr. Intell. Syst.*, Aug. 2008, pp. 434–438.

[27] A. Schmitz, P. Maiolino, M. Maggiali, L. Natale, G. Cannata, and G. Metta, "Methods and technologies for the implementation of large-scale robot tactile sensors," *IEEE Trans. Robot.*, vol. 27, no. 3, pp. 389–400, Jun. 2011.

[28] Y. Hasegawa, H. Sasaki, M. Shikida, K. Sato, and K. Itoigawa, "Magnetic actuation of a micro-diaphragm structure for an active tactile sensor," in *Proc. IEEE Int. Symp. Micro-Nanomechatron. Human Sci. Symp. Micro-Nanomechatron. Inf.-Based Soc.*, Oct./Nov. 2004, pp. 99–104.

[29] M. Goka, H. Nakamoto, and S. Takenawa, "A magnetic type tactile sensor by GMR elements and inductors," in *Proc. IEEE/RSJ Int. Conf. Intell. Robots Syst.*, Oct. 2010, pp. 885–890.

[30] R. R. Reston and E. S. Kolesar, "Pressure-sensitive field-effect transistor sensor array fabricated from a piezoelectric polyvinylidene fluoride film," in *Proc. Annu. Int. Conf. IEEE Eng. Med. Biol. Soc.*, vol. 3, Nov. 1989, pp. 918–919.

[31] K. Hosoda, "Robot finger design for developmental tactile interaction: Anthropomorphic robotic soft fingertip with randomly distributed receptors," in *Proc. Embodied Artif. Intell.*, vol. 3139, 2003, pp. 219–230.

[32] Y. Tanaka, M. Tanaka, and S. Chonan, "Development of a sensor system for measuring tactile sensation," in *Proc. IEEE Conf. Sensors*, Oct. 2006, pp. 554–557.

[33] R. S. Dahiya, M. Valle, G. Metta, L. Lorenzelli, and A. Adami, "Piezoelectric oxide semiconductor field effect transistor touch sensing devices," *Appl. Phys. Lett.*, vol. 95, no. 3, p. 034105, 2009.

[34] R. S. Dahiya *et al.*, "Towards tactile sensing system on chip for robotic applications," *IEEE Sensors J.*, vol. 11, no. 12, pp. 3216–3226, Dec. 2011.

[35] H. Ishiguro and S. Nishio, "Building artificial humans to understand humans," *J. Artif. Organs*, vol. 10, no. 3, pp. 133–142, 2007.

[36] S. Takamuku, G. Gómez, K. Hosoda, and R. Pfeifer, "Haptic discrimination of material properties by a robotic hand," in *Proc. IEEE Int. Conf. Develop. Learn.*, Jul. 2007, pp. 1–6.

[37] M. Lee and H. Nicholls, "Review article tactile sensing for mechatronics—A state of the art survey," *Mechatronics*, vol. 9, no. 1, pp. 1–31, 1999.

[38] M. Ohka, H. Kobayashi, and Y. Mitsuya, "Sensing characteristics of an optical three-axis tactile sensor mounted on a multi-fingered robotic hand," in *Proc. IEEE/RSJ Int. Conf. Intell. Robots Syst.*, Aug. 2005, pp. 493–498.

[39] Y. Ohmura, Y. Kuniyoshi, and A. Nagakubo, "Conformable and scalable tactile sensor skin for curved surfaces," in *Proc. IEEE Int. Conf. Robot. Autom.*, May 2006, pp. 1348–1353.

[40] J. Heo, C. Han, and J. Lee, "Evaluation of the tactile sensor element using the microbending optical fiber sensors," in *Proc. Int. Conf. Sens. Technol.*, 2007, pp. 74–78.

[41] B. L. Hutchings, A. R. Grahn, and R. J. Petersen, "Multiple-layer cross-field ultrasonic tactile sensor," in *Proc. IEEE Int. Conf. Robot. Autom.*, vol. 3, May 1994, pp. 2522–2528.

[42] M.-Y. Cheng *et al.*, "Design and fabrication of an artificial skin using PI-copper films," in *Proc. IEEE Int. Conf. Micro Electro Mech. Syst.*, Jan. 2007, pp. 389–392.

[43] T. Yoshikai *et al.*, "Development of robots with soft sensor flesh for achieving close interaction behavior," *Adv. Artif. Intell.*, vol. 2012, pp. 1–27, Jan. 2012.

[44] R. S. Dahiya and M. Valle, "Tactile sensing for robotic applications," in *Sensors, Focus on Tactile, Force and Stress Sensors*. Vukovar, Croatia: InTech, 2008, ch. 15, pp. 289–304.

[45] R. Russell, *Robot Tactile Sensing*, R. Russell, Ed. Englewood Cliffs, NJ, USA: Prentice-Hall, 1990.

[46] P. Dario *et al.*, "Biologically-inspired microfabricated force and position mechano-sensors," in *Proc. Int. Symp. Mech. Plants, Animals Their Environ.*, 2000, 20 pp.

[47] D. De Rossi and E. Scilingo, "Skin-like sensor arrays," in *Encyclopedia of Sensors*. Valencia, CA, USA: American Scientific Pub., 2006, pp. 535–556.

[48] M. Cutkosky, R. Howe, and W. Provancher, "Force and tactile sensors," in *Handbook of Robotics*. Berlin, Germany: Springer-Verlag, 2008, ch. 19, pp. 455–476.

[49] R. Wijesiriwardana, K. Mitcham, W. Hurley, and T. Dias, "Capacitive fiber-meshed transducers for touch and proximity-sensing applications," *IEEE Sensors J.*, vol. 5, no. 5, pp. 989–994, Oct. 2005.

[50] A. Ueno, Y. Akabane, T. Kato, H. Hoshino, S. Kataoka, and Y. Ishiyama, "Capacitive sensing of electrocardiographic potential through cloth from the dorsal surface of the body in a supine position: A preliminary study," *IEEE Trans. Biomed. Eng.*, vol. 54, no. 4, pp. 759–766, Apr. 2007.

[51] M. Maggiali, G. Cannata, P. Maiolino, G. Metta, M. Randazzo, and G. Sandini, "Embedded distributed capacitive tactile sensor," in *Proc. Mechatron. Forum Biennial Int. Conf.*, 2008, 5 pp.

[52] A. Schmitz, M. Maggiali, M. Randazzo, L. Natale, and G. Metta, "A prototype fingertip with high spatial resolution pressure sensing for the robot iCub," in *Proc. IEEE-RAS Int. Conf. Humanoid Robots*, Dec. 2008, pp. 423–428.

[53] J. C. Doll, S.-J. Park, and B. L. Pruitt, "Design optimization of piezoresistive cantilevers for force sensing in air and water," *J. Appl. Phys.*, vol. 106, no. 6, pp. 064310-1–064310-12, 2009.

[54] M. Shimojo, A. Namiki, M. Ishikawa, R. Makino, and K. Mabuchi, "A tactile sensor sheet using pressure conductive rubber with electrical-wires stitched method," *IEEE Sensors J.*, vol. 4, no. 5, pp. 589–596, Oct. 2004.

[55] T. Mouri, H. Kawasaki, K. Yoshikawa, J. Takai, and S. Ito, "Anthropomorphic robot hand: Gifu hand III," in *Proc. Int. Conf. Comput. Appl.*, 2002, pp. 1288–1293.

[56] M. W. Strohmayr, H. P. Saal, A. H. Potdar, and P. van der Smagt, "The DLR touch sensor I: A flexible tactile sensor for robotic hands based on a crossed-wire approach," in *Proc. IEEE Int. Conf. Intell. Robots Syst.*, Oct. 2010, pp. 897–903.

[57] H. Iwata and S. Sugano, "Human-robot-contact-state identification based on tactile recognition," *IEEE Trans. Ind. Electron.*, vol. 52, no. 6, pp. 1468–1477, Dec. 2005.

[58] Y.-H. Wen, G. Y. Yang, V. J. Bailey, G. Lin, W. C. Tang, and J. H. Keyak, "Mechanically robust micro-fabricated strain gauges for use on bones," in *Proc. IEEE/EMBS Special Topic Conf. Microtechnol. Med. Biol.*, May 2005, pp. 302–304.

[59] K. Yongdae, K. Youngdeok, L. Chulsub, and K. Sejin, "Thin polysilicon gauge for strain measurement of structural elements," *IEEE Sensors J.*, vol. 10, no. 8, pp. 1320–1327, Aug. 2010.

[60] A. M. Lebar, G. F. Harris, J. J. Wertsch, and H. Zhu, "An optoelectric plantar 'shear' sensing transducer: Design, validation, and preliminary subject tests," *IEEE Trans. Rehabil. Eng.*, vol. 4, no. 4, pp. 310–319, Dec. 1996.

[61] Y. Yamada, M. Morizono, U. Umetani, and T. Takahashi, "Highly soft viscoelastic robot skin with a contact object-location-sensing capability," *IEEE Trans. Ind. Electron.*, vol. 52, no. 4, pp. 960–968, Aug. 2005.

[62] A. Ataollahi, P. Polygerinos, P. Puangmali, L. D. Seneviratne, and K. Althoefer, "Tactile sensor array using prismatic-tip optical fibers for dexterous robotic hands," in *Proc. IEEE/RSJ Int. Conf. Intell. Robots Syst.*, Oct. 2010, pp. 910–915.

[63] J. Rossiter and T. Mukai, "An LED-based tactile sensor for multi-sensing over large areas," in *Proc. IEEE Conf. Sensors*, Oct. 2006, pp. 835–838.

[64] M. Feneberg, K. Thonke, T. Wunderer, F. Lipski, and F. Scholz, "Piezoelectric polarization of semipolar and polar GaInN quantum wells grown on strained GaN templates," *J. Appl. Phys.*, vol. 107, no. 10, pp. 103517-1–103517-6, 2010.

[65] M. Willatzen, B. Lassen, L. C. L. Y. Voon, and R. V. N. Melnik, "Dynamic coupling of piezoelectric effects, spontaneous polarization, and strain in lattice-mismatched semiconductor quantum-well heterostructures," *J. Appl. Phys.*, vol. 100, no. 2, pp. 024302-1–024302-6, 2006.

[66] H. Ishiguro, "Android science: Towards a new cross-disciplinary framework," in *Proc. CogSci Workshop, Toward Soc. Mech. Android Sci.*, 2005, pp. 1–6.

[67] T. Noda, T. Miyashita, H. Ishiguro, and N. Hagita, "Super-flexible skin sensors embedded on the whole body, self-organizing based on haptic interactions," in *Proc. Robot., Sci. Syst.*, 2008, pp. 294–301.

[68] C. Dong-June, C.-T. Rim, S. Kim, and Y. K. Kwak, "High sensitivity inductive sensing system for position measurement," in *Proc. IEEE Conf. Instrum. Meas. Technol.*, May 2000, pp. 595–599.

[69] A. Drumea, P. Svasta, and M. Blejan, "Modelling and simulation of an inductive displacement sensor for mechatronic systems," in *Proc. 33rd Int. Spring Seminar Electron. Technol.*, May 2010, pp. 304–307.

[70] X. Ding, K. Kuribayashi, and T. Hashida, "Development of a new type tactile sensor using micro electromagnetic coil for human robot," in *Proc. IEEE Int. Symp. Micromechatron. Human Sci.*, Oct. 2000, pp. 181–187.

[71] K. S. Jaichandar and E. A. M. Garcia, "Intelli-sense bed patient movement sensing and anti-sweating system for bed sore prevention in a clinical environment," in *Proc. Int. Conf. Commun. Signal Process.*, Dec. 2011, pp. 1–5.

[72] H. Ruser, "Smartlow-cost weather sensor as an example for 'multi-component' sensors," in *Proc. IEEE Int. Conf. Multisensor Fusion Integr. Intell. Syst.*, Sep. 2006, pp. 559–564.

[73] J. H. Cho, M. Kothare, and M. G. Arnold, "Reconfigurable multi-component sensors built from MEMS payloads carried by micro-robots," in *Proc. IEEE Sensors Appl. Symp.*, Feb. 2010, pp. 15–19.

[74] Y. Kato and T. Mukai, "Tactile sensor without wire and sensing element in the tactile region using new rubber material," in *Sensors, Focus on Tactile, Force and Stress Sensors*. Rijeka, Croatia: InTech, 2008, ch. 22, pp. 399–408.

[75] H. Alirezaei, A. Nagakubo, and Y. Kuniyoshi, "A tactile distribution sensor which enables stable measurement under high and dynamic stretch," in *Proc. IEEE Symp. 3D User Inter.*, Mar. 2009, pp. 87–93.

[76] A. Yao and M. Soleimani, "A pressure mapping imaging device based on electrical impedance tomography of conductive fabrics," *Sensor Rev.*, vol. 32, no. 4, pp. 310–317, 2012.

[77] D. S. Tawil, D. C. Rye, and M. Velonaki, "Improved EIT drive patterns for a robotics sensitive skin," in *Proc. Austral. Conf. Robot. Autom.*, 2009, 10 pp.

[78] H. Liu, X. Song, J. Bimbo, L. Seneviratne, and K. Althoefer, "Surface material recognition through haptic exploration using an intelligent contact sensing finger," in *Proc. IEEE/RSJ Int. Conf. Intell. Robots Syst.*, Oct. 2012, pp. 52–57.

[79] F. L. Hammond, III, R. K. Kramer, Q. Wan, R. D. Howe, and R. J. Wood, "Soft tactile sensor arrays for micromanipulation," in *Proc. IEEE/RSJ Int. Conf. Intell. Robots Syst.*, Oct. 2012, pp. 25–32.

[80] A. Yao, C. L. Yang, J. K. Seo, and M. Soleimani, "EIT-based fabric pressure sensing," *Comput. Math. Methods Med.*, vol. 2013, Jan. 2013, Art. ID 405325.

[81] B. Robins, F. Amirabdollahian, Z. Ji, and K. Dautenhahn, "Tactile interaction with a humanoid robot for children with autism: A case study analysis involving user requirements and results of an initial implementation," in *Proc. IEEE Int. Symp. Robot Human Interact. Commun.*, Sep. 2010, pp. 704–711.

[82] D. S. Tawil, D. Rye, and M. Velonaki, "Interpretation of the modality of touch on an artificial arm covered with an EIT-based sensitive skin," *Int. J. Robot. Res.*, vol. 31, no. 13, pp. 1627–1641, 2012.

[83] M. D. Cooney, S. Nishio, and H. Ishiguro, "Recognizing affection for a touch-based interaction with a humanoid robot," in *Proc. IEEE/RSJ Int. Conf. Intell. Robots Syst.*, Oct. 2012, pp. 1420–1427.

[84] D. Silvera-Tawil, D. Rye, and M. Velonaki, "Interpretation of social touch on an artificial arm covered with an EIT-based sensitive skin," *Int. J. Soc. Robot.*, vol. 6, no. 4, pp. 489–505, Nov. 2014.

[85] R. P. Henderson and J. G. Webster, "An impedance camera for spatially specific measurements of the thorax," *IEEE Trans. Biomed. Eng.*, vol. BME-25, no. 3, pp. 250–254, May 1978.

[86] R. J. Lytle and K. A. Dines, "Impedance camera: A system for determining the spatial variation of electrical conductivity," Lawrence Livermore Lab., Univ. California, Berkeley, CA, USA, Tech. Rep. UCRL-52413, 1978.

[87] C. S. Koh, M.-K. Kim, H.-K. Jung, S.-Y. Hahn, and B.-S. Suh, "Electric resistivity tomography for geophysical inverse problems," *IEEE Trans. Magn.*, vol. 33, no. 2, pp. 1852–1855, Mar. 1997.

[88] R. W. Stacey, "Electrical impedance tomography," Stanford Geothermal Program, Stanford Univ., Stanford, CA, USA, Tech. Rep. SGP-TR-182, 2006.

[89] J.-H. Yu, "Study on algorithm of ERT for voidage measurement of two-phase flow," in *Proc. IEEE Int. Conf. Mach. Learn. Cybern.*, vol. 4, Aug. 2007, pp. 2401–2404.

[90] R. Mann, "ERT imaging and linkage to CFD for stirred vessels in the chemical process industry," in *Proc. IEEE Int. Workshop Imag. Syst. Techn.*, May 2009, pp. 218–222.

[91] C. Tan and F. Dong, "Gas-water two-phase flow regime identification with feature fusion from an ERT system and a V-cone meter," in *Proc. IEEE Int. Workshop Imag. Syst. Techn.*, May 2009, pp. 307–312.

[92] D. C. Barber and A. D. Seagar, "Fast reconstruction of resistance images," *Clin. Phys. Physiol. Meas.*, vol. 8, no. 4A, pp. 47–54, Nov. 1987.

[93] B. H. Brown and A. D. Seagar, "The Sheffield data collection system," *Clin. Phys. Physiol. Meas.*, vol. 8, no. 4A, pp. 91–97, 1987.

[94] A. Adler and R. Guardo, "Electrical impedance tomography: Regularized imaging and contrast detection," *IEEE Trans. Med. Imag.*, vol. 15, no. 2, pp. 170–179, Apr. 1996.

[95] I. Frerichs, G. Hahn, T. Schröder, and G. Hellige, "Electrical impedance tomography in monitoring experimental lung injury," *Intensive Care Med.*, vol. 24, no. 8, pp. 829–836, 1998.

[96] M. Cheney, D. Isaacson, and J. C. Newell, "Electrical impedance tomography," *Soc. Ind. Appl. Math.*, vol. 41, no. 1, pp. 85–101, 1999.

[97] S. Heinrich, H. Schiffmann, A. Frerichs, A. Klockgether-Radke, and I. Frerichs, "Body and head position effects on regional lung ventilation in infants: An electrical impedance tomography study," *Intensive Care Med.*, vol. 32, no. 9, pp. 1392–1398, 2006.

[98] X. Shi, X. Dong, W. Shuai, F. You, F. Fu, and R. Liu, "Pseudo-polar drive patterns for brain electrical impedance tomography," *Physiol. Meas.*, vol. 27, no. 11, pp. 1071–1080, 2006.

[99] C. C. Barber, B. H. Brown, and I. L. Freeston, "Imaging spatial distributions of resistivity using applied potential tomography," *Electron. Lett.*, vol. 19, no. 22, pp. 933–935, Oct. 1983.

[100] M. Vauhkonen, "Electrical impedance tomography and prior information," Ph.D. dissertation, Dept. Appl. Phys., Kuopio Univ., Kuopio, Finland, 1997.

[101] B. Brandstatter, "Jacobian calculation for electrical impedance tomography based on the reciprocity principle," *IEEE Trans. Magn.*, vol. 39, no. 3, pp. 1309–1312, May 2003.

[102] B. M. Graham and A. Adler, "A nodal Jacobian inverse solver for reduced complexity EIT reconstructions," *Int. J. Inf. Syst. Sci.*, vol. 2, no. 4, pp. 453–468, 2006.

[103] C. Gómez-Laberge and A. Adler, "Direct EIT Jacobian calculations for conductivity change and electrode movement," *Physiol. Meas.*, vol. 29, no. 6, pp. S89–S99, 2008.

[104] T. Dai, "Image reconstruction in EIT using advanced regularization frameworks," Ph.D. dissertation, Dept. Syst. Comput. Eng., Carleton Univ., Ottawa, ON, Canada, 2008.

[105] J. Hadamard, *Lectures on Cauchy's Problem in Linear Partial Differential Equations*, vol. 37. London, U.K.: Yale Univ. Press, 1923.

[106] J. Noor, "Electrical impedance tomography at low frequencies," Ph.D. dissertation, Faculty Sci., Univ. New South Wales, Sydney, Australia, 2007.

[107] P. Silvester and R. Ferrari, Eds., *Finite Elements for Electrical Engineers*. Cambridge, U.K.: Cambridge Univ. Press, 1996.

[108] G. Nikishkov, "Introduction to the finite element method," Univ. Aizu, Aizuwakamatsu, Japan, Tech. Rep., 2009.

[109] A. Elsanadedy, "Application of electrical impedance tomography to robotic tactile sensing," M.S. thesis, School Mech. Eng., Carleton Univ., Ottawa, ON, Canada, 2012.

[110] D. S. Tawil, "Artificial skin and the interpretation of touch for human-robot interaction," Ph.D. dissertation, School Aerosp., Mech. Mechatron. Eng., Univ. Sydney, New South Wales, Australia, 2012.

[111] P.-O. Persson and G. Strang, "A simple mesh generator in MATLAB," *Soc. Ind. Appl. Math.*, vol. 46, no. 2, pp. 329–345, 2004.

[112] C. Moler, Ed., *Numerical Computing With MATLAB*. Natick, MA, USA: MathWorks Inc., 2004. [Online]. Available: http://www.mathworks.com/moler

[113] W. R. B. Lionheart, "EIT reconstruction algorithms: Pitfalls, challenges and recent developments," *Physiol. Meas.*, vol. 25, no. 1, pp. 125–142, 2004.

[114] N. Polydorides and H. McCann, "Electrode configurations for improved spatial resolution in electrical impedance tomography," *Meas. Sci. Technol.*, vol. 13, no. 12, pp. 1862–1870, 2002.

[115] M. Soleimani, "Image and shape reconstruction methods in magnetic induction and electrical impedance tomography," Ph.D. dissertation, School Math., Univ. Manchester, Manchester, U.K., 2005.

[116] E. J. Woo, P. Hua, J. G. Webster, and W. J. Tompkins, "A robust image reconstruction algorithm and its parallel implementation in electrical impedance tomography," *IEEE Trans. Med. Imag.*, vol. 12, no. 2, pp. 137–146, Jun. 1993.

[117] T. J. Yorkey, J. G. Webster, and W. J. Tompkins, "Comparing reconstruction algorithms for electrical impedance tomography," *IEEE Trans. Biomed. Eng.*, vol. BME-34, no. 11, pp. 843–852, Nov. 1987.

[118] B. M. Graham and A. Adler, "Objective selection of hyperparameter for EIT," *Physiol. Meas.*, vol. 27, no. 5, pp. S65–S79, May 2006.

[119] M. Cheney, D. Isaacson, J. C. Newell, S. Simske, and J. Goble, "NOSER: An algorithm for solving the inverse conductivity problem," *Int. J. Imag. Syst. Technol.*, vol. 2, no. 2, pp. 66–75, 1990.

[120] A. Adler and W. R. B. Lionheart, "Uses and abuses of EIDORS: An extensible software base for EIT," *Physiol. Meas.*, vol. 27, no. 5, pp. S25–S42, 2006.

[121] D. S. Tawil, D. Rye, and M. Velonaki, "Touch modality interpretation for an EIT-based sensitive skin," in *Proc. IEEE Int. Conf. Robot. Autom.*, May 2011, pp. 3770–3776.

[122] J.-W. Liu and F. Dong, "Electrical resistance tomography based on the single drive electrode method," in *Proc. IEEE Int. Conf. Mach. Learn. Cybern.*, vol. 1, Aug. 2004, pp. 632–637.

[123] J. J. Cilliers, W. Xie, S. J. Neethling, E. W. Randall, and A. J. Wilkinson, "Electrical resistance tomography using a bi-directional current pulse technique," *Meas. Sci. Technol.*, vol. 12, no. 8, pp. 997–1001, 2001.

[124] H. Alirezaei, A. Nagakubo, and Y. Kuniyoshi, "A highly stretchable tactile distribution sensor for smooth surfaced humanoids," in *Proc. 7th IEEE-RAS Int. Conf. Humanoid Robots*, Nov./Dec. 2007, pp. 167–173.

[125] D. Isaacson, "Distinguishability of conductivities by electric current computed tomography," *IEEE Trans. Med. Imag.*, vol. 5, no. 2, pp. 91–95, Jun. 1986.

[126] E. Demidenko, A. Hartov, N. Soni, and K. D. Paulsen, "On optimal current patterns for electrical impedance tomography," *IEEE Trans. Biomed. Eng.*, vol. 52, no. 2, pp. 238–248, Feb. 2005.

[127] J. Kaipio, A. Seppänen, A. Voutilainen, and H. Haario, "Optimal current patterns in dynamical electrical impedance tomography imaging," *Inverse Problems*, vol. 23, no. 3, pp. 1201–1214, 2007.

[128] P. Hua, E. J. Woo, J. G. Webster, and W. J. Tompkins, "Iterative reconstruction methods using regularization and optimal current patterns in electrical impedance tomography," *IEEE Trans. Med. Imag.*, vol. 10, no. 4, pp. 621–628, Dec. 1991.

[129] D. G. Gisser, D. Isaacson, and J. C. Newell, "Current topics in impedance imaging," *Clin. Phys. Physiol. Meas.*, vol. 8, no. 4A, pp. 39–46, 1987.

[130] R. D. Cook, G. Saulnier, D. G. Gisser, J. C. Goble, J. C. Newell, and D. Isaacson, "ACT3: A high-speed, high-precision electrical impedance tomograph," *IEEE Trans. Biomed. Eng.*, vol. 41, no. 8, pp. 713–722, Aug. 1994.

[131] M. Cheney and D. Isaacson, "Distinguishability in impedance imaging," *IEEE Trans. Biomed. Eng.*, vol. 39, no. 8, pp. 852–860, Aug. 1992.

[132] A. Borsic, B. M. Graham, A. Adler, and W. Lionheart, "*In vivo* impedance imaging with total variation regularization," *IEEE Trans. Med. Imag.*, vol. 29, no. 1, pp. 44–54, Jan. 2010.

[133] D. B. Geselowitz, "An application of electrocardiographic lead theory to impedance plethysmography," *IEEE Trans. Biomed. Eng.*, vol. BME-18, no. 1, pp. 38–41, Jan. 1971.

[134] N. J. Avis and D. C. Barber, "Image reconstruction using non-adjacent drive configurations," *Physiol. Meas.*, vol. 15, no. 2A, pp. A153–A160, 1994.

[135] C. Xu *et al.*, "Comparison of drive patterns for single current source EIT in computational phantom," in *Proc. IEEE Int. Conf. Bioinform. Biomed. Eng.*, May 2008, pp. 1500–1503.

[136] L. M. Heikkinen, M. Vauhkonen, T. Savolainen, and J. P. Kaipio, "Modelling of internal structures and electrodes in electrical process tomography," *Meas. Sci. Technol.*, vol. 12, no. 8, pp. 1012–1019, 2001.

[137] J. L. Wheeler, W. Wang, and M. Tang, "A comparison of methods for measurement of spatial resolution in two-dimensional circular EIT images," *Physiol. Meas.*, vol. 23, no. 1, pp. 169–176, 2002.

[138] A. Adler *et al.*, "GREIT: A unified approach to 2D linear EIT reconstruction of lung images," *Physiol. Meas.*, vol. 30, no. 6, pp. S35–S55, 2009.

[139] M. Soleimani, C. Gómez-Laberge, and A. Adler, "Imaging of conductivity changes and electrode movement in EIT," *Physiol. Meas.*, vol. 27, no. 5, pp. S103–S113, 2006.

David Silvera-Tawil was born in Mexico City, Mexico. He received the B.E. (Hons.) degree in electronics and telecommunications from Universidad Iberoamericana, Mexico City, in 2002, the M.Eng.Stud. (Hons.) degree in mechatronics, in 2007, and the Ph.D. degree in artificial skin and human–robot interaction from the University of Sydney, Sydney, NSW, Australia, in 2012. He is currently a Post-Doctoral Fellow with the Creative Robotics Laboratory, University of New South Wales, Sydney, Australia. His long-term research interests are in the area of human–robot interaction, social robotics, and assistive technologies. His aim is for humans and robots to share the same physical space, interacting and communicating in similar, intuitive ways and working, helping, and cooperating as peers to achieve both shared and independent goals. His current research contributes toward expanding the understanding of human behavior in social environments and improving social and affective human–robot interaction. His previous research involved interactive interfaces, remote laboratories for distance learning, and artificial robotic skin and touch interpretation in human–robot interaction.

David Rye works in embedded and applied control of machinery, and in the design and implementation of computer-controlled systems. Although his background is originally in mechanical engineering, he works principally on computerized machinery, electronics, software, and systems design. He has conducted industrial research and development projects related to automation and control of machinery, including shipboard and container-handling cranes and the system design and experimental validation of autonomous vehicles. Since 2003, he has worked on human–robot interaction in a media arts context. In 2006, he co-founded, with M. Velonaki, the Centre for Social Robotics at the Australian Centre for Field Robotics, University of Sydney, Sydney, NSW, Australia. He is also internationally recognized as a pioneer in the introduction and development of university teaching in mechatronics, having instituted the first Australian Bachelor of Engineering in Mechatronics in 1990.

Manuchehr Soleimani received the B.Sc. degree in electrical engineering and the M.Sc. degree in biomedical engineering from the Sharif University of Technology, Tehran, Iran, in 1996 and 1999, respectively, and the Ph.D. degree in inverse problems and electromagnetic tomography from the University of Manchester, Manchester, U.K., in 2005. From 2005 to 2007, he was a Research Associate with the School of Materials, University of Manchester, where he developed a range of wearable devices and biomedical textile. In 2007, he joined the Department of Electronic and Electrical Engineering, University of Bath, Bath, U.K., where he was a Research Associate and became an Assistant Professor in 2008 and an Associated Professor in 2013. He has authored over 200 journal papers, review papers, book chapters, and papers in conference proceedings. He holds several patents. In 2011, he established the Engineering Tomography Laboratory, University of Bath, where he leads a group of 15 Ph.D. students and post-doctoral researchers in various areas of tomographic imaging.

Mari Velonaki has been a researcher in Robotics and Interactive Media Art since 1997. She has created intellectually and emotionally engaging human–machine interfaces that incorporate movement, speech, touch, breath, electrostatic charge, artificial vision, light, and text. In 2003, she began to work with robotics, initiating and leading a major ARC Linkage Art/Science Research Project in collaboration with robotics scientists at the Australian Centre for Field Robotics, University of Sydney, Sydney, NSW, Australia. In 2006, she co-founded the Centre for Social Robotics, Sydney, a centre dedicated to cross-disciplinary research into human–robot interaction. She was a recipient of the Australia Council for the Arts Visual Arts Fellowship in 2007, and an ARC Discovery Grant and Queen Elizabeth II Fellowship in 2009. She is the founder and Director of the Creative Robotics Laboratory, National Institute of Experimental Arts, University of New South Wales, Sydney, Australia.